

Proton Scattering of Neutron-Rich He-Isotopes in Inverse Kinematics A New Setup for the High Momentum Transfer Measurements

F. Aksouh¹, O.A. Kisselev^{1,2}, A. Bleile¹, O.V. Bochkarev³, L.V. Chulkov³,
D. Cortina-Gil¹, A.V. Dobrovolsky^{1,2}, P. Egelhof¹, H. Geissel¹, M. Hellström¹, N.B. Isaev²,
B.G. Komkov², M. Mátos¹, F.V. Moroz², G. Münzenberg¹, M. Mutterer⁴, V.A. Mylnikov²,
S.R. Neumaier¹, V.N. Pribora³, D.M. Seliverstov², L.O. Sergueev², A. Shrivastava¹,
K. Sümmerer¹, H. Weick¹, M. Winkler¹ and V.I. Yatsoura²

¹ GSI, ² PNPI Gatchina, ³ Kurchatov Institute Moscow, ⁴ TU Darmstadt

Proton elastic scattering at intermediate energies of around 700 MeV/u is well suited for determining radii and nuclear matter distributions of halo nuclei such as ${}^6,8\text{He}$ [1] and ${}^{11}\text{Li}$ [2]. The first measurement on the ${}^6,8\text{He}$ nuclei in inverse kinematics has been performed at low momentum transfer up to $|t| = 0.05$ (GeV/c)² using gaseous hydrogen as proton target. From theoretical investigations [3] a high sensitivity on the inner part of the nuclear matter distributions is predicted when extending the $p^6\text{He}$ and $p^8\text{He}$ elastic cross section measurement to the higher momentum transfer region ($|t| = 0.1 - 0.4$ (GeV/c)²). Calculations based on Glauber theory show that the position of the first diffraction minimum depends on the shape of the density distribution, and is within the model strongly correlated to the core radius of the halo nucleus. We conclude, that a measurement of the angular distribution at higher momentum transfer should yield unambiguous information about the intrinsic structure of these nuclei. In addition, also inelastic reaction channels may be investigated.

A recent experiment has been carried out at GSI in October 2000. The ${}^6,8\text{He}$ beams were obtained via fragmentation of an ${}^{18}\text{O}$ primary beam of about 10^{10} ions/spill. The projectile fragments were separated by the FRS yielding secondary beam intensities of 5×10^3 - 10^5 ions/s with an energy of about 700 MeV/u. The experimental setup installed in cave B is shown in fig.1. A forward spectrom-

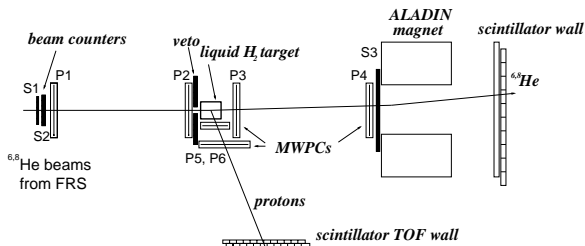


Figure 1: Schematic drawing of the S174 experimental setup.

eter has been used for tracking and identifying the projectile nuclei and for separating the elastic events from the inelastic and break-up channels. It also provided the signal for the first level trigger. This spectrometer consisted of four X-Y position sensitive multiwire proportional chambers (MWPC) P1-P4 with cathode strip channel-by-channel readout, several beam scintillators (S1-S3, Veto), the ALADIN magnet and a position sensitive scintillator wall behind. The proportional chambers had rather high position resolution of 100-150 μm and an efficiency close to 100%. A second position sensitive scintillator wall was used to measure ΔE and time-of-flight of the recoil pro-

tons. The second level trigger used the signals from two proportional chambers (P5, P6) detecting and tracking the recoil protons. The essential difference with respect to the previous ${}^6,8\text{He}$ experiment [1] was, that the high recoil proton energies up to $E_p = 160$ MeV allowed to replace the gaseous H_2 target by a 600 mg/cm² liquid H_2 target. This target and the cryogenic device used for the experiment were constructed at CEA, Saclay. The cylindrical target had a total length of 120 mm and an inner diameter of 30 mm. The use of a liquid hydrogen target allows to decrease significantly the background as compared to similar experiments with CH_2 targets.

The data analysis is still in progress. To illustrate the quality of the acquired data, X-position spectra obtained with the MWPC P4 in the field free region before the ALADIN magnet for two different experimental conditions are displayed in fig.2. The spectrum on the left side was taken

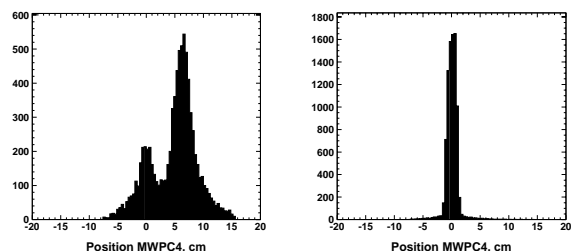


Figure 2: X position spectra from the MWPC P4 obtained for $p^6\text{He}$ scattering for two different experimental conditions (see text).

for the case the second level trigger (that demands recoil protons) being switched on. The one shown on the right side was obtained for the case the second level trigger was switched off, thus displaying the profile of the unscattered beam. The dominant peak in the spectrum on the left side clearly reflects the distribution of elastically and inelastically scattered ${}^6\text{He}$ projectiles, whereas the peak around $X=0$ is due to the unscattered beam particles contributing to the background. From these online raw spectra we conclude that practically background free data on elastic and inelastic $p^6,8\text{He}$ scattering will be available after the final analysis taking into account all measured parameters.

References

- [1] G.D. Alkhazov *et al.*, Phys. Rev. Lett. 78 (1997) 2313.
- [2] S.F. Neumaier *et al.*, to be published in Nucl. Phys. A, A.V. Dobrovolsky *et al.*, this report.
- [3] L.V. Chulkov *et al.*, Nucl. Phys. A 587 (1995) 291.

Progress in the Optimization of the FOCAL Crystal Spectrometer

H.F. Beyer⁹, J. Bojowald⁴, G. Borchert⁴, F. Bosch⁹, W. Bröchle⁹, M. Czanta⁹, R.D. Deslattes¹, E. Förster³, A. Freund², A. Gumberidze⁹, A. Hamacher⁴, J. Hoszowska², P. Indelicato⁶, H.-J. Kluge⁹, Chr. Kozhuharov⁹, D. Liesen⁹, B. Lommel⁹, T. Ludziejewski⁸, X. Ma⁹, B. Manil⁶, I. Mohos⁴, D. Protić⁴, A. Simionovici², Th. Stöhlker⁹, C. Striezel⁷, S. Toleikis⁹, N. Trautmann⁵, J. Tschischgale³, A.H. Walenta⁷, O. Wehrhan³

¹National Institute of Standards and Technology, Gaithersburg, Maryland 20899, USA

²European Synchrotron Radiation Facility (ESRF), F-38043 Grenoble, France

³Institut für Optik und Quantenelektronik, Friedrich Schiller-Universität, D-07743 Jena, Germany

⁴FZ Jülich, Institut für Kernphysik, Germany

⁵Institut für Kernchemie, Universität Mainz, D-55128 Mainz, Germany

⁶Université P. et M. Curie, Lab. Kastler Brossel, F-75252 Paris Cédex, 05 France

⁷Universität Siegen, Fachbereich 7 Physik, D-57068 Siegen, Germany

⁸The Andrzej Soltan Institute for Nuclear Studies, 05-400 Swierk, Poland

⁹GSI Darmstadt

The FOCAL x-ray spectrometer is being developed for the accurate measurement of the 1s Lamb shift in one-electron heavy ions. In the **FO**cussing **C**ompensated **A**symmetric **L**aué geometry part of the possible wavelength resolution is traded off in favor of an increased sensitivity through a broadening of the crystal rocking curve [1].

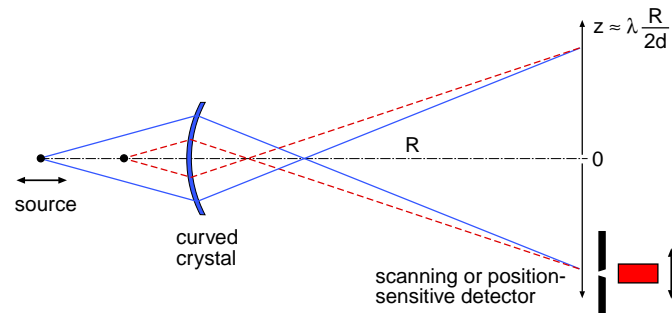


Figure 1: Principle of the x-ray optical arrangement used for systematic tests of the FOCAL spectrometer. The x-ray path is shown for one wavelength at two different locations of the gamma-ray source.

The spectrometer has been set up on a test bench where several systematic investigations were performed during the past year. Figure 1 schematically shows the x-ray optical arrangement with a movable x-ray source parked at two different positions. The x rays are dispersed along the positive and negative z axis in a symmetric way where the displacement is approximately proportional to the wavelength. Spectra obtained from a ^{169}Yb source were recorded either with a scanner equipped with a narrow slit and a conventional Ge(i) detector or with the new micro-strip germanium detector under development [2]. Recording the x-ray spectra for a couple of different gamma-ray lines and for a range of source-to-crystal distances, it is possible to map out the x-ray optics and the performance and possible deviations of the crystal from its ideal cylindrical shape. Up to now such tests have solely been made with the scanner. A first test of the spectrometer in combination with the new micro-strip detector was made for a fixed source-to-crystal separation

amounting to 300 mm compared to 2 m as the nominal radius of curvature of the crystal.

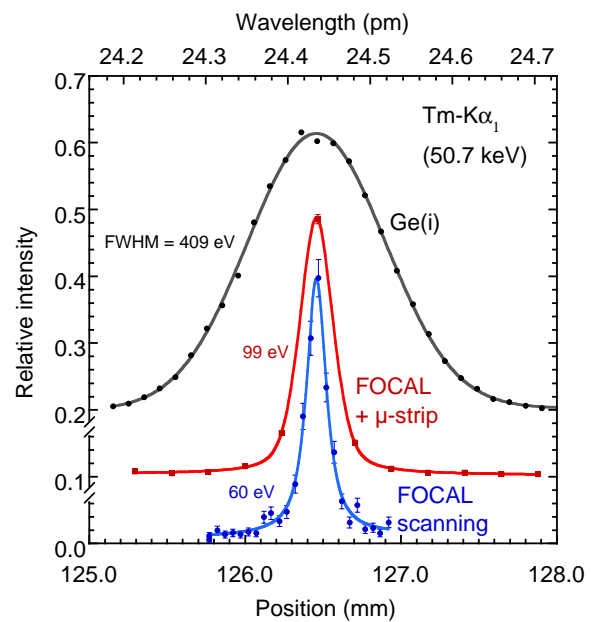


Figure 2: The wavelength profile of the $\text{Tm-K}\alpha_1$ line measured as the pulse-height spectrum of a conventional solid-state Ge(i) detector or measured with the FOCAL spectrometer equipped either with a position-sensitive micro-strip detector or in scanning mode.

Figure 2 compares measurements of the $\text{Tm-K}\alpha_1$ line near 50.7 keV from the decay of ^{169}Yb with FOCAL operated in scanning mode or with the micro-strip detector attached. For reference the pulse-height spectrum of the conventional Ge(i) is also included. The line widths of 150 μm (60 eV) and 250 μm (99 eV) for the scanner and for the micro-strip detector, respectively, are consistent with the expectations taking into account the slit width of 50 μm and the 235 μm combined stripe and gap width. Additionally the natural line width of 30 eV and the

contribution from the rocking curve amounting to 40 eV have to be considered.

The present position sensitive detector has an area of $47 \times 23.4 \text{ mm}^2$ and is structured with 200 stripes, each $200 \mu\text{m}$ wide, which are separated by grooves of $35 \mu\text{m}$ width. This prototype will soon be replaced by an upgraded version optimized in order to cover a substantial fraction of the astigmatic height of the spectral lines and to be position sensitive in *two* dimensions. This will be realized by etching grooves into both the front and rear surface of the germanium crystal.

For characterizing the silicon crystal, the source-to-crystal separation was varied between 260 and 550 mm. Gamma-rays near 50, 63 and 110 keV were reflected from different spots on the crystal that are offset by a distance ranging from ± 8 to ± 28 mm from the centre of the crystal. The results from these measurements revealed deviations of the curvature from the ideal cylindrical shape. In figure 3 the observed line widths are plotted as a function of the calculated position on the crystal. Going from the centre towards the edges of the crystal the width strongly increases. Presumably this is caused by the mechanical stress introduced in the bending device. We will try to reduce this effect by using only the inner region of a larger crystal and by a change of the design of the crystal bender.

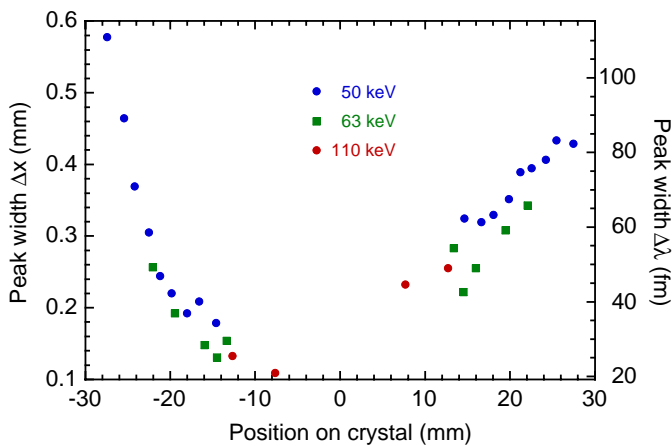


Figure 3: Observed line width for three different x-ray energies and for reflections occurring at different locations on the crystal.

For a more stringent test the crystal curvature was measured with synchrotron radiation at the optics beamline of the ESRF in Grenoble. There the white synchrotron beam was collimated down to a width of 0.5 mm with the secondary slits located at some 40 m downstream the bending magnet. The measurement setup is schematically illustrated in figure 4.

In a first step two *flat* silicon crystals having the same dimensions as the curved one, namely $80 \times 40 \times 1.5 \text{ mm}^3$, were prepared for the 220 reflection in the Laue case with an asymmetry angle of $\chi = 2^\circ$. The crystals were aligned using a scintillator detector and reflections were found in the non-dispersive (+1,-1) and dispersive (+1,+1) geometry by rotating the second crystal relative to the first one. The setup was tuned to a Bragg angle of 3.034° corresponding to approximately 61 keV x-ray energy. The first crystal, serving as a monochromator, was not touched anymore throughout the rest of the experiment.

In a second step the second crystal of the arrangement was replaced by the curved crystal to be tested and subsequently the (+1,-1) reflection was found. The x-ray beam incident on

the curved crystal was shifted horizontally, in an approximately parallel way, in steps of 2 mm by means of an according movement of the secondary collimating slits in front of the experimental setup. For each translation Δx of the incident beam the Bragg reflection on the curved crystal was found by rotating the curved crystal.

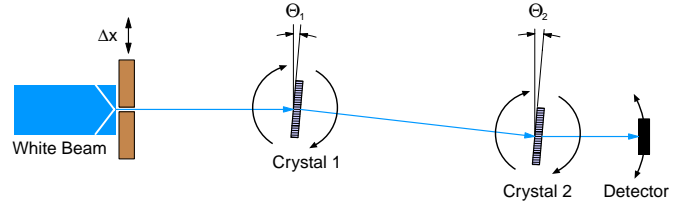


Figure 4: The two-crystal set up used at the optics beamline at the ESRF.

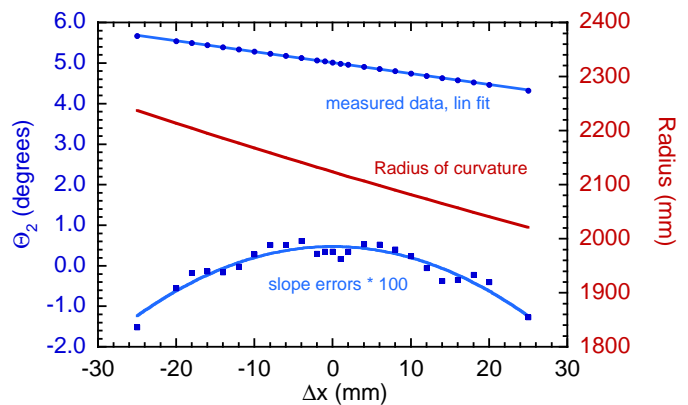


Figure 5: Curvature results obtained with the measurement illustrated in figure 4. From the deviations of the angular positions from a strict linear behavior the variation of the bending radius across the crystals long dimension is obtained.

The relation between the angular position θ_2 of the reflection maximum and the translation Δx is plotted in figure 5. For an ideal cylinder a straight line is expected. Small deviations from the linear fit are shown in the figure as *slope errors*, i.e. as the differences between the angular data measured and the linear fit. For better visibility the slope errors were multiplied by a factor of 100. From the smooth curve through the slope errors the variation of the radius of curvature across the crystals long dimension has been derived which is also plotted in figure 5. The $\pm 5\%$ variation of the radius for a ± 25 -mm excursion on the crystal is consistent with optical measurements using the crystals reflecting surfaces.

The present results were obtained for a trace centered on the crystal. As soon as an improved version of the bent crystal is assembled we will complement the curvature measurements tracing the crystal also in the anticlastic direction.

References

- [1] H.F. Beyer, Nucl. Instrum. Methods. A **400** (1997) 137; H.F. Beyer et al., GSI Scientific Report 1999, p. 209.
- [2] Th. Stöhlker et al., GSI Scientific Report 1999, p. 206. D. Protić et al., IEEE Trans. Nucl. Sci. to be published.

PHELIX, a Petawatt High Energy Laser for Heavy-Ion Experiments

Th. Kühl¹, J. Alvarez¹, B. Becker-de Mos¹, R. Bock¹, S. Borneis¹, H. Brand¹, D. Browning⁴, C. Bruske¹, K. Brück³, J. Caird⁴, E. Dewald², C. Haefner¹, D.H.H. Hoffmann², H.-J. Kluge¹, D. Marx¹, P. Neumayer¹, M. Perry⁵, H. Powell⁴, I. Reinhard¹, M. Roth¹, W. Seelig², A. Tauschwitz², R. Wilcox⁴

¹Gesellschaft für Schwerionenforschung mbH, Planckstr.1, 64291 Darmstadt, Germany

²TU Darmstadt, Schlossgartenstr. 7, 64283 Darmstadt, Germany

³Universität Mainz, Staudingerweg 7, 55099 Mainz

⁴Lawrence Livermore National Laboratory, 7000 East Ave., Livermore, CA 94550

⁵General Atomics, P.O. Box 85608, San Diego, CA 92186

<http://www.gsi.de/phelix>

The laser building for PHELIX [1], started with the ground-breaking in December 1999, was finished in August. It was inaugurated as part of the celebration of 30 years of GSI by the German Federal Minister für Bildung und Forschung, E. Buhlman and the Hessian State Minister für Wissenschaft und Kunst, R. Wagner (Fig.1)



Fig. 1.: Inauguration of the laser building August 25th 2000 by the German Bundesminister für Bildung und Forschung, E. Buhlman (with scissors) and the Hessian Staatsminister für Wissenschaft und Kunst, R. Wagner

On the ground floor the building houses the 500 m² laser hall for the main amplifier and the laser front-ends and an additional preparation space of 60 m². These rooms are equipped as class-10000 clean rooms. A mirror tower, solidly anchored to the 90 cm-thickness foundation plate, will lead the beam up to the beam switchyard on the second floor. Here also the pulsed power bay, the control-room, and a 60 m² class-100 clean room for the assembly of laser optics are situated. The building was engineered to allow operation and target delivering of the laser at the typical level of ground vibrations found under operation of the accelerator and the installations in the accelerator halls.

In parallel to the construction, preparations of the laser installations were made. The design parameters of the main amplifier [2][3] were verified by calculations performed at the Lawrence Livermore National Laboratory in Livermore, California, and at the CEA laboratory in Le Barp, near

Bordeaux. The conclusion was to foresee 5 amplifier heads within the 2-pass amplifier. This will allow to create pulses with up to 1 Kilojoule in this first part of the amplifier, and to reach values necessary for Petawatt operation with only this section. In the booster amplifier, isolated by a Faraday isolator, 5 more amplifiers are planned to increase the energy level to 5 Kilojoules for 5 ns to 10 ns pulses. The floor plan of the laser installation is shown in Fig. 2.

This makes it possible to send pulses up to the 1-Kilojoule level directly to the experiments, and to inject into the booster amplifier section only for the high-energy option.

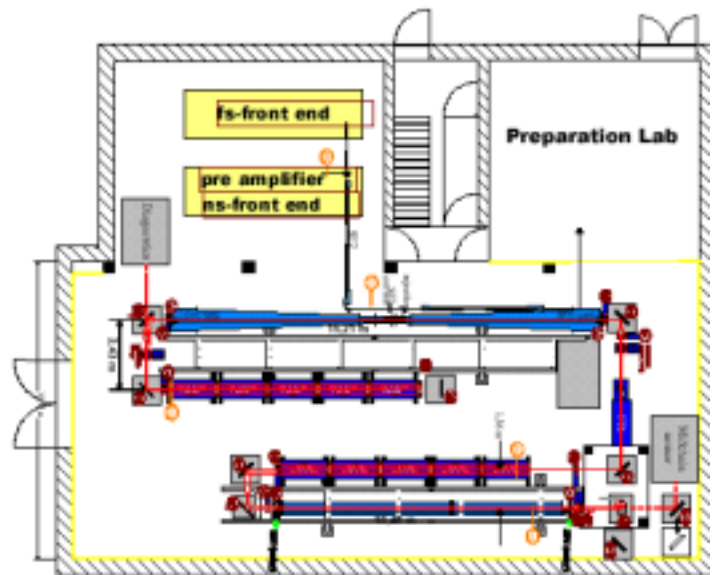


Fig. 2.: Modified lay-out of the PHELIX chain.

Shortly after the laser building became utilizable the fs-front-end components were shipped and installed. This system consists of a commercial femto-second oscillator, pumped by a diode-pumped Nd:YVO₄ laser, and two custom-built regenerative amplifiers. The first parts of the PHELIX nanosecond front-end have been assembled and tested. The ns-frontend basically consists of seven individual parts, the fiber-oscillator, a fiber-based double pass amplifier, an amplitude modulator to tailor the temporal pulse shape, a phase modulator to provide additional bandwidth, a fail safe system to protect the bigger laser components, a ring regenerative amplifier and a beam shaping section to modulate the spatial laser beam profile. Within 2000 the first three parts have been built and

tested in close collaboration with the Lawrence Livermore National Laboratory. The PHELIX design is based on a modified prototype which is to be used for the National Ignition Facility and similar to the Z-beamlet laser system at Sandia. Except for the the ring regenerative amplifier and the beam shaping section the PHELIX ns-frontend is based on fiber technology. This provides stable and robust operation without much further alignment and maintenance. The fiber components are housed in 19" racks that can be placed anywhere inside the laser building.

The oscillator module provides a stable, continuous laser beam of 15 mW, single mode, at 1053 nm delivered by a laser diode pumped Y-doped fiber laser. It is injected into a double pass fiber amplifier, which is shown in Fig. 3.



Fig. 3.: The 19" fiber-optics double-pass amplifier of the ns-frontend.

The laser beam is chopped by an acousto-optic modulator into individual pulses of 100 ns length and amplified to several nanojoules (corresponding to a few Watts peak power) with the aid of a laser diode pumped Y-doped fiber and a Bragg grating used as a fiber end-mirror.

These pulses are then sent to the amplitude modulator section. The modulator consists of two fiber based Mach-Zehnder interferometers made of Li-Niobate. If a low voltage electrical signal is applied to one arm of each of the interferometers, it changes the refractive index of the material and therefore causes a modulation of the exiting laser radiation. The electrical input signal is converted into temporal shaping of the laser pulse. The temporal resolution of the modulator is better than 100 picoseconds, mainly limited by the driving electrical circuit.

For most of the future experiments planned for PHELIX, nanosecond temporal resolution is required. Thus, and due to the varying experimental conditions, a highly versatile electrical pulse generator (arbitrary waveform generator, AWG) is used. Individually designed electrical pulses can be generated in the computer control system and will be transformed into PHELIX laser pulses using the AWG. Fig. 4. shows long term stability test results for the system (oscillator, double pass and modulator). An excellent energy stability was found even though the whole system was housed not in a temperature

controlled environment like it will be in the PHELIX building. Furthermore the performance of the modulator section was tested as seen in Fig. 5. The electrical input signal from the

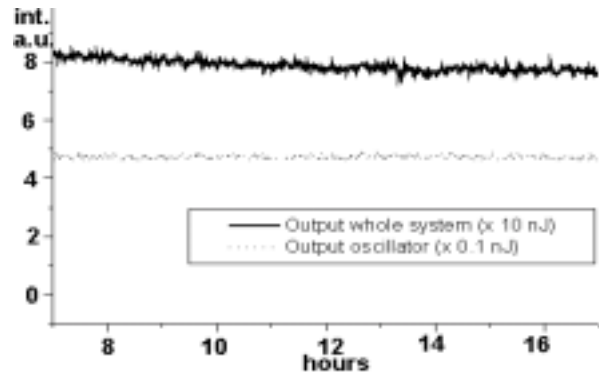


Fig. 4.: PHELIX ns-frontend long term energy stability.

AWG is shown together with the optical output of the laser beam measured by a fast photodiode. The chosen pulse shape was similar to a 'Haan' type pulse that is used in laser fusion experiments. The test results show a excellent response of the electro-optical system to the input signals. A total contrast ratio of 60 dB has been obtained, which is sufficient for further amplification up to the kilojoule level.

The components have been shipped to GSI and were re-activated successfully. The remaining parts, namely the phase

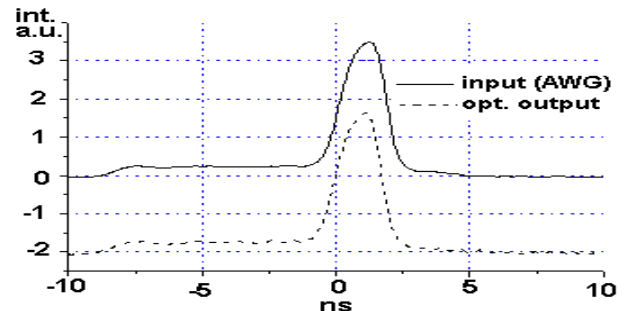


Fig. 5.: Performance test of the modulator section.

modulator and the fail safe system are currently under construction at Livermore and will become operational within the year 2001. The regenerative amplifier is operational at GSI and will be placed into the PHELIX building for detailed performance tests.

Parts for the preamplifier section which will amplify these pulses up to the 10 Joule level are under preparation together with the Lawrence Livermore Laboratory.

In conclusion, the first parts of the PHELIX front-ends are operational with excellent performance and will be coupled to the following amplifier sections early in the year 2001.

References

- [1] PHELIX Project, GSI-98-10 Report, December 1998
- [2] PHELIX - A Petawatt High-Energy Laser for Heavy-Ion Experiments, R. Bock et al., Inertial Fusion Sciences and Applications 99, C. Labaune, W.J. Hogan, K.A. Tanaka Eds., Elsevier Publishing, Paris, Amsterdam, Lausanne, New York, Oxford, Shannon, Tokyo (2000) 703
- [3] PHELIX – ein Petawatt-Hoch-Energie-Laser, Th. Kühl, Phys. Bl. 5 (2000) 49

A Zero-Degree Electron Spectrometer for (e,2e) Spectroscopy at the ESR

S. Hagmann^{1,2,3}, R. Moshhammer^{3,4}, J. Ullrich^{3,4}, Th. Stöhlker², H.Kollmus^{2,3,4}, R.Mann²

¹J.R.Macdonald Lab., Dept. of Physics, KSU, Manhattan, KS,USA; ²GSI-Darmstadt;
³Fakultät für Physik, Universität Freiburg; ⁴MPI- Heidelberg

The jet target of the ESR provides unprecedented conditions to study atomic collision dynamics in the realm of relativistic ion beams. A complete rebuild of the target environment has broadened the range of possible experiments considerably. Besides x-ray spectroscopy, now recoil-ion momentum and electron spectroscopy experiments can be conducted.

Presently we are implementing a magnetic electron spectrometer at the ESR storage ring dedicated to 0^0 -electron spectroscopy in collisions of stored ions with gaseous and cluster targets at the gasjet target region: we will focus on high resolution electron spectroscopy of Rydberg states of the projectile and on electrons in the projectile continuum, emphasizing electron impact ionization (e,2e) of the projectile. The spectrometer expands the possibilities of the new longitudinal reaction microscope (RM)[1] for kinematically complete experiments with relativistic ions in the ESR.

In recent experiments the fundamental process of Coulomb ionization of atoms and ions has been investigated in kinematical complete experiments using the reaction microscope[1,2]. The break-up of atoms, i.e. Single and Multiple Ionization (SI, MI) for weak and strong perturbing fields and perturbation times down to 10^{-18} sec have been studied[2] with respect to the dependence of the emission characteristics of electrons on the momentum transfer \mathbf{k} from the dipolar (small \mathbf{k}) to the binary regime (large \mathbf{k}).

Applying the reaction microscope we have begun, first at low collision energies, to investigate for the first time kinematically complete electron impact ionization (e,2e) of ions[2] which is inaccessible to standard crossed beam techniques due to insufficient luminosity.

(e,2e) collision channels in ion-atom collisions are characterized by simultaneous correlated emission of a fast electron with $v_e \approx v_{\text{Projectile}}$ in a narrow cone around the projectile direction and a slow electron, mostly in the forward hemisphere. In the reaction microscope all collision products are detected with near 4π efficiency; for collision energies well below 4AMeV mapping both, the fast and the slow electron onto one multihit capable detector still results in an acceptable momentum resolution. The collision plane of the ionizing collisions is then event-wise reconstructed.

This technique gains orders of magnitude in luminosity over standard crossed beam techniques which are restricted to one collision plane predefined by detector geometry with correspondingly low efficiency. This way one opens up the avenue to electron impact ionization of few-electron highly charged ions over the entire Z range.

However, for collision energies above $\approx 4\text{AMeV}$, it is not acceptable to map the fast and the slow electron onto one multihit capable detector. For this reason an independent magnetic spectrometer is necessary at ESR energies which guides electrons emitted into a narrow cone around the beam direction onto a position sensitive detector and which allows to reconstruct the initial momentum of the fast electron. The

design criteria for construction of the instrument are a) separate electrons from the flood of secondary products with minimum interference with the ESR beam, b) analyze electrons emitted in a direction near 0^0 close to the beam over a wide range of momenta including $v_e \approx v_{\text{Projectile}}$ up to specific projectile energies of 560AMeV; in non-position sensitive mode a momentum resolution $\Delta p/p = 10^{-3}$ is desired, c) in position sensitive mode, reconstruct the emission direction of the electron in the target zone after transport from the jet-target in the ESR to the detector.

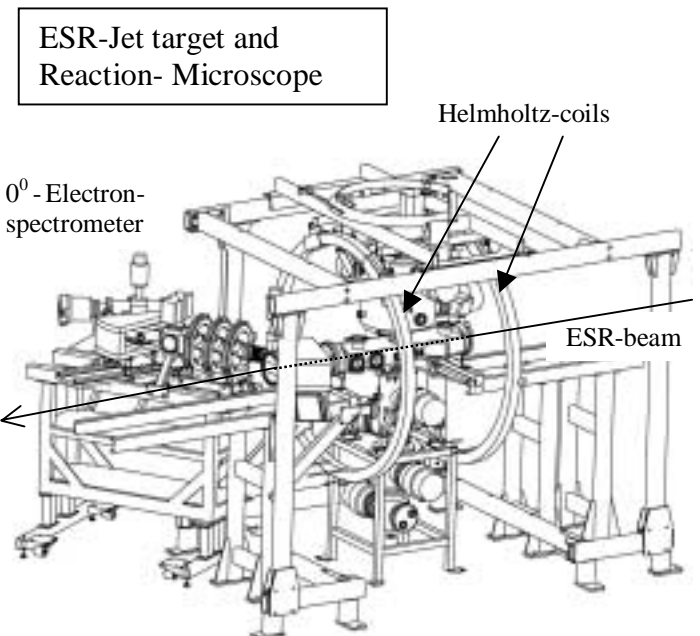


Fig. 1: ESR with supersonic jet target environment and downstream 0^0 magnetic electron spectrometer

The design chosen using beam trajectory calculations with the Mirko code is of D-T-D type and covers a solid angle of $4 \cdot 10^{-4}$ sr. A 60^0 magnetic dipole of bending radius 200mm, with an aperture of vertically 100mm and horizontally 250mm as required by the ESR, 940mm from the target zone and just downstream of the target chamber is followed by a magnetic quadrupole triplet of 80mm aperture and a second dipole, identical to the first one. This is followed by a pair of horizontal slits and 2D position sensitive electron detector. As an option an open hyperpure Ge detector for independent analysis of the energy of electrons and identification of other particles potentially transmitted through the spectrometer will be installed during commissioning of the spectrometer as the low energy spectrum of secondary particles produced in the ESR target zone is currently not known.

[1] J. Ullrich et al., J.Phys.B30(1997)2917

[2] R.Moshhammer et al, this Annual Report

LabVIEW@GSI

D. Beck, H.Brand, Poppensieker, K. Wunderle, DVEE, GSI Darmstadt

DVEE started the evaluation of LabVIEW (National Instruments, NI¹) as a tool for the development of slow control systems for experiments of small and medium size in 1999. During the past years the use of LabVIEW in research and industry has strongly increased. For GSI, the main advantages of using NI software are the following: First, NI provides both hard- and software. By this, the time consuming development of low level drivers is not an issue any more. Second, it provides efficient tools for the development of graphical user interfaces (GUIs). Finally, LabVIEW, being a graphical programming language, eases the software development even for inexperienced programmers. As a result, software development with LabVIEW becomes more efficient and less time consuming for many cases. The maintenance and further development of existing LabVIEW based systems is rather easy.

LabVIEW is the method of choice for software development when PC hardware with Microsoft operating systems can be used. Even real time applications can be implemented using embedded systems from NI. Interfaces to access VXI/VME and CAMAC hardware from a PC based system is made possible by hardware provided by NI. This gives access to legacy hardware that is widely used in research.

LabVIEW is also available for Linux and the number of supported hardware interfaces is continuously growing. However, porting the LabVIEW applications itself to other operating systems like LynxOS, which are not supported by NI, is almost excluded.

At GSI, DV&EE is involved in several LabVIEW projects required for physics experiments:

- TargetScanner², Target Laboratory [1].
- SHIPTRAP³, Atomic Physics
- Life time measurements in Cave A, Atomic Physics
- PHELIX⁴, Atomic Physics
- Detector test, Detector Laboratory

For these projects different hardware and field-busses are supported.

- NI Flex- and Value-Motion, with a MOVTEC power amplifier for stepper motors
- NI IMAQ⁵ to acquire images from different analog and digital cameras
- CAN bus to control high voltage modules (iseg)
- GPIB to control local and remote GPIB devices
- NI FieldPoint to control digital and analog I/O via Ethernet
- Profibus via an interface from COMSOFT
- CAMAC and VME

All this hardware can easily be accessed via LabVIEW, which is an integrated development environment. LabVIEW also

includes powerful libraries and add-on toolkits that help to efficiently set-up control systems:

- SQL- and Internet-Toolkit to access data bases and networks.
- Statistical Process Control for quality assurance of continuous processes
- PID and Fuzzy-Toolkit for closed loop control
- Advanced IMAQ Vision library for image processing and analysis
- Data Logging and Supervisory Control (former BridgeVIEW) for alarm and event handling, online and historical trending and security

We use these tools to develop prototype applications and instrument drivers in LabVIEW. Most of these projects are maintained using a build-in Source Code Control System that is part of the LabVIEW environment. More detailed information can be found on the web, <http://www-wnt.gsi.de/LabVIEW>.

The EPICS ActiveX Channel Access Server library [2] for LabVIEW was successfully evaluated for HADES⁶.

The Data Logging and Supervisory Control Module (former Bridgeview) for LabVIEW provides OPC client and server functionality that can be used to set-up communication with commercial OPC servers like the one from COMSOFT for a Profibus controller.

There are two more NI software packages to mention. LabWindows/CVI is the C based analogue to LabVIEW and ComponentWorks++ provides C++ libraries and GUI elements which can be used with other C/C++ development environments like Microsoft Visual Studio.

To provide CAMAC access over the network we used those packages to implement the ESONE client library on Windows via a C/C++ DLL. The MBS⁷ [3] provides the ESONE server. For this purpose the ONC RPC software package was used. It implements SUN Remote Procedure Calls for Windows using the XDR format (External Data Representation. Microsoft RPC uses NDR format, Network Data Representation, which is not compatible with XDR). A wrapper library for LabVIEW is supported too. VME is also easily accessible via a VME-MXI-2 Controller from NI.

To summarize, LabVIEW from NI provides powerful software tools for the implementation of PC based control systems. At GSI it is currently mainly used for small and medium sized experiments.

References

[1] H.Brand et. al., "Project Targetscanner – A Status Report", GSI Annual Report 2000

[2] Kai-Uwe Kasemir, <http://mesa53.lanl.gov/lansce8/epics/PC/>

[3] H.G. Essel und N. Kurz, „The General Purpose Data Acquisition System MBS“, IEEE TRANSACTION ON NUCLEAR SCIENCE, VOL. 47, NO. 2, APRIL 2000

⁶ <http://www-hades.gsi.de>

⁷ Multi Branch System

¹ <http://www.ni.com>

² <http://www-wnt.gsi.de/TargetScanner>

³ <http://www-aix.gsi.de/~shiptrap>

⁴ <http://www-aix.gsi.de/~phelix>

⁵ IMAQAcquisition

On-line Analysis in MBS 3.0

H. G. Essel, N. Kurz
DVEE, GSI Darmstadt

Current Status

Since there are powerful VME processor boards on the market and MBS [1] event builders may run also on standard PCs under LynxOS, analyzing events on-line becomes a reasonable option. This on-line analysis may be useful for several tasks:

1. *Software filter*: Analysis decides which events to store.
2. *Monitoring*: Analysis controls if the experiment equipment works correctly.
3. *Histogramming*: Sometimes it may not be necessary to store the event data, if histograms can be accumulated on-line.

In all cases the data need not to be transferred over networks and the analysis processes all events. MBS 3.0 has integrated the full L^A [2] histogram package except the IDL graphics part. Visualization can be done by any GSI histogram client (L^A , Origin, Go4viewer, MBS GUI), as shown in figures 1 and 2.

Developing an On-line Analysis

An MBS on-line analysis can be completely developed on Linux, AIX, or VMS using the L^A tools. With the GUI one can set up the histograms. Then L^A generates all necessary include files, templates, startup procedures and makefiles for LynxOS. After copying these files to an MBS node, the makefile generates a user specific MBS collector program.

With the identical sources the L^A user program can be made on the other platforms. The analysis can be tested off-line or on-line. If it runs correctly it can again be distributed to the MBS node, remade, and run inside the collector.

Differences to L^A

Because the event loop in the MBS collector is different from L^A , the event analysis function in MBS (f_mbs_anal) has different arguments than the L^A function (f_anal). One can, however, use the MBS function also in L^A .

Data bases are transient in L^A but persistent in MBS. In both cases bases can be dumped, exchanged, and restored. In the startup procedures of MBS the base might be attached if it already exists or restored, if not.

In MBS there is another task, the Histogram Manager, to control the data bases, i.e. manage histograms and conditions. This task also runs a histogram server thread providing remote access to the histograms.

In MBS, the analysis function f_mbs_anal is called event by event in the collector after the acquisition has been started. This calling can be switched on or off by commands.

Compatibility to L^A

Data bases containing histograms and conditions can be exchanged between all platforms. All commands managing histograms or conditions are the same. Therefore command procedures can be exchanged.

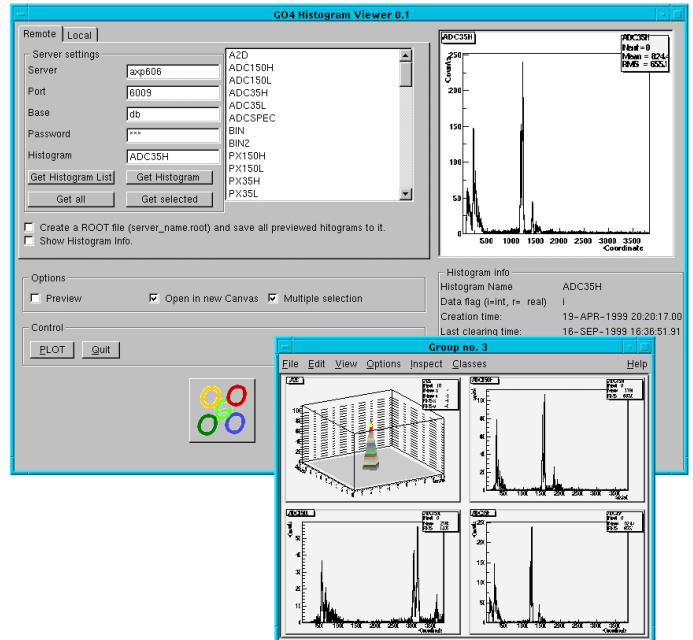


Figure 1: Go4viewer based on ROOT.

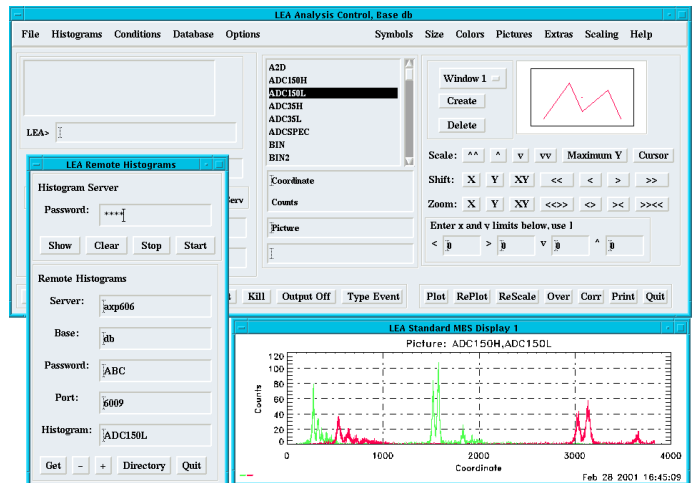


Figure 2: L^A as histogram client.

Actual information on further developments can be found on <http://daq.gsi.de> or <http://lea.gsi.de>.

References

- [1] H.G.Essel and N.Kurz, "The General Purpose Data Acquisition System MBS", IEEE Trans. NS, Vol. 47, No. 2, (April 2000), pp. 337
- [2] H.G.Essel, "Lean Analysis with L^A ", GSI Report 1999 (2000), p 233

Go4: Multitasking Multithreaded Class Library

J. Adamczewski, M. Al-Turany, H. G. Essel, H. Göringer
DVEE, GSI Darmstadt

At the beginning of the GSI Online-Offline-Object-Oriented analysis project GO4, the principle of a multi threaded analysis based on the ROOT framework [1] had already been demonstrated by a first prototype [2]. In the following phase, the software has been redesigned completely using UML tools such as *RationalRose 2000* [3] and, more recently, *Together 4.2* [4], in connection with the *Sniff++* development environment [5].

Go4 Thread Manager

The *Go4ThreadManager* package provides foundation and service classes to launch any number of named threads within a ROOT application. It is based on the ROOT TThread library which had been updated in the course of the first Go4 prototype. The *Go4ThreadManager* implements the concept of runnable classes (like JAVA) which the user may specialize by inheritance for any job without changing the Go4 thread classes themselves.

Go4 Task Handler

The first goal of the Go4 kernel was to control several independent, distributed analysis clients (slaves) from one user interface server task (master). Therefore, the *Go4TaskHandler* package and the related service packages (*Go4Socket*, *Go4Queue*, *Go4CommandsBase*, and *Go4StatusBase*) were designed for such inter task connections.

The client communicates with the server via three sockets (data, command, and status channel). Each of these channels is processed by a dedicated thread and is buffered against the user's application by means of a thread safe template queue. The entire communication setup is encapsulated within the *Go4TaskHandler* class.

Exchange of information between server and clients is done by command objects and by status objects. Here we use a command design pattern [6] with an invoker singleton, and a modified memento pattern, respectively. Commands created by the server may be either sent to one of the remote clients, or added to a local command queue to be executed in a local thread preventing the blocking of the GUI.

Status objects are created by the clients and are sent to the server which may e.g. display the current analysis status. Additionally, any named ROOT object created by an analysis client (e.g. a histogram) can be sent to the GUI via the task handler data channel.

A new client process may either be launched from an existing GUI server process and can be added to the list of clients; or the client may be started independently and may request a new connection to the server process at any time.

Test of Go4 Multitasking

As a first test of the *Go4TaskHandler* package, we built an example client (subclass of TGo4ClientTask), and an example display (subclass of TGo4ServerTask). The client has two additional threads working on an example application (the actual analysis later on) . The client status information is sent to the server regularly by thread one, while thread two executes commands and processes the analysis (here a random histogram

fill). The server has a simple GUI control panel, a ROOT canvas and a status window.

Two server threads wait to display any client objects appearing at the status and data queues, respectively. Pressing a GUI button, a histogram is requested from the currently selected client by command, sent to the server and drawn on the canvas. This example was running successfully over >24 hours with 1 server task connected to 7 client tasks on 4 different nodes, which promises a stable operation of the task handler system.

Go4 Viewer

In addition to the design of the Go4 framework, the *Go4Viewer* is being built as a first tool for visualization and interactive manipulation of histograms, ntuples and root TTrees. Based on native ROOT GUI classes it features access to data from different sources: from GSI histogram servers like LeA, GOOSY and MBS, from local root or paw files, and from the GSI mass storage system using the root TRFIO classes. Histograms and ntuples from any data sources are converted on the fly to ROOT file format and may be analyzed later by all means of the ROOT system.

Conclusions and Outlook

The Go4 Task handler package might be a flexible tool for any kind of distributed tasks using the ROOT environment. In contrast to the existing parallel root facility PROOF (which is specialized for parallel processing on the same dataset), the *Go4TaskHandler* is capable of controlling independent clients with threaded applications, required both for non blocking online analysis or slow control jobs.

The next step will be the implementation of the actual analysis framework, containing abstract interfaces for the event related classes, a dynamic list which will keep and process online generated histogram objects, and a system of analysis condition classes. Here we will still benefit from the first Go4 prototype experiences.

The *Go4Viewer* may be a test bed for the future GUI layout, until the first test analysis of the Go4 framework will produce viewable data.

Documentation of Go4 can be found at <http://go4.gsi.de>.

References

- [1] <http://root.cern.ch>
- [2] *Status of ROOT Based Analysis System Go4*, J.Adamczewski, H.G.Essel, H.Göringer, M. Hemberger, N. Kurz, M.Richter; GSI scientific report 1999, p.232
- [3] <http://www.rational-software.de>
- [4] <http://www.togethersoft.com>
- [5] <http://www.windriver.com/products/html/sniff.html>
- [6] *Design Patterns: Elements of Reusable Object-Oriented Software*, E.Gamma, R.Helm, R.Johnson, J.Vlissides ; Addison-Wesley 1999

Grid Tests and Developments

Ingo Giese, Peter Malzacher
GSI Darmstadt

The DataGrid project

The computing model for the storage, management, simulation, reconstruction, distribution, and analysis of the data of the four LHC experiments (ALICE, ATLAS, CMS, and LHCb) consists of two key elements[1]:

- A multi-tier hierarchical model of regional centres developed by the MONARC (Models of Networked Analysis at Regional Centres for LHC experiments) group [2].
- Grid[3] software will be used as flexible middleware for the secure, coordinated access to the resources distributed worldwide.

After an about one year preparation phase, the EU funded DataGrid project[4] started in January 2001: A three year development and test phase to demonstrate the feasibility of the grid approach to the LHC computing challenge. The major development projects are:

- Data grid services to provide workload management, scheduling, and data movement as well as monitoring services across institutional boundaries.
- Fabric management including network infrastructure, cluster and mass storage management.
- A production quality test bed using scientific applications from high energy physics, earth observation, and biology.

Globus Installation

To explore grid tools and to be ready to use the first test bed of the DataGrid project, release 1.1.3 of the Globus Toolkit[5] has been installed on the central Linux and AIX clusters of GSI. Globus offers the basic protocols, services, and APIs (application programmer interfaces) to use geographically and organizationally dispersed computing resources:

- GRAM: The Globus Resource Allocation Manager. It unites grid machines, providing a common user interface to the different batch systems.
- GIS: The Grid Information Service. It provides a common interface to discover the properties of grid resources.
- GSI: The Grid Security Infrastructure, a library for providing generic security services for applications that will be run on the grid.

Users on all central Linux and AIX machines at GSI can use the Globus services to submit processes to other grid sites. The main advantage is a single worldwide Globus user id. A test machine has been configured as gatekeeper to our local batch system LSF.

A major computational challenge for the ALICE collaboration during 2001 will be the simulation for the physics performance report. After successful explorations between different centres, it is planned to use Globus tools for parts of these massive productions.

ROOT and Grid

AliRoot, the ALICE off-line framework for simulation, reconstruction, and analysis is built on ROOT[6], a set of OO

frameworks widely used in high energy and nuclear physics to build data acquisition, simulation, and analysis systems. The main features of ROOT are:

- The ability to handle and analyse large amounts of data in an efficient way.
- The built-in CINT C++ interpreter, which allows for a fast prototyping, since the command language, scripting language, and the implementation language are all C++.
- A rich set of classes including histogramming, fitting, and visualization.

To build the basic infrastructure for one of the long term use cases of ALICE - interactive distributed analysis on the grid - we started to interface two Globus APIs to ROOT.

PROOF, the Parallel ROOT Facility, allows to send work via wide area networks to a master server which distributes it to slave servers, collects the results, and sends the results back to the client. A prototype of using the grid security infrastructure to authenticate the client to the servers has been developed. It will be put into the ROOT distribution soon. The same mechanism can be used for remote file access via TNetFile and rootd or for the coming TFTP class.

Wide area distributed analysis requires careful selection of the resources used, based on available CPUs, network bandwidth, and load as well as data location. Neither manual configuration nor defaults are acceptable. Manual configuration requires deep knowledge of the remote system that an average user does not possess. Even the best defaults cannot fit to the ever changing resources. Decisions should be made at run-time based on the structure and state of the computing environment as well as the needed resources. Therefore the second Globus API we want to use in ROOT is the grid information service. The basic protocol for this information service is LDAP (Lightweight Directory Access Protocol)[7]. We developed a small C++ layer on top of the LDAP C API. The next step is to integrate it in ROOT along the lines of the SQL interface classes.

References

- [1] Report of the Steering Group of the LHC Computing Review, CERN/LHCC/2001-004.
- [2] MONARC Phase 2 report, CERN/LCB/2000-001.
- [3] Ian Forster, Carl Kesselman, Steven Tuecke: The Anatomy of the Grid, Enabling Scalable Virtual Organizations, to appear: Int. J. Supercomputer Applications, 2001.
- [4] <http://www.datagrid.cnr.it/>.
- [5] Ian Foster, Carl Kesselman, Globus: A Toolkit-Based Grid Architecture. In: Ian Forster, Carl Kesselman (Eds), The GRID: Blueprint for a new Computing Infrastructure, (1999) pages 259-278. See also <http://www.globus.org>.
- [6] Rene Brun and Fons Rademakers, *ROOT - An Object Oriented Data Analysis Framework*, NIM A389 (1997) 81-86. See also <http://root.cern.ch/>.
- [7] RFC 1823: The LDAP Application Programming Interface.

Project Targetscanner – A Status Report

Holger Brand, Klaus Poppensieker, Willi Hartmann, Birgit Kindler,
Josef Klemm, Bettina Lommel, Jutta Steiner

Introduction: With the Fragment Separator (FRS) at GSI radioactive-heavy-ion beams can be prepared to study properties of and reactions with relativistic exotic nuclei. The quality of this beam depends crucially on the perfection of the energy degraders which are necessary for slowing down the heavy ions according to their mass and charge, and therefore, act as variable ion-optical devices. The accuracy of the energy adjustment and the perfection of isotope separation depends on the thickness of the degrader parts as a lateral function.

The actual cause for the project Target Scanner was the plan to replace the degrader units of the FRS. In a first step S1 will be replaced, the other units will follow little by little. Among others the degraders at S1 consists in the moment of two aluminium wedges with ~230mmx500mm in dimension. Several years ago the thickness distribution of these parts was measured fully manual with about one measuring point every 5 mm. That meant positioning, measuring, reading and writing down the values for about 4000 times per wedge. Since the new degraders have to be made a lot more precisely also the thickness measurement has to be more precise. We have to measure at least once every mm that means at least a 100.000 data points per part.

That is the reason for setting up the Target Scanner, a device for measuring and evaluating the thickness of parts variable in geometry and size as a lateral function fully automatically via a PC. The target scanner works purely mechanically, which means that there are no special requirements concerning the properties of the surfaces to be measured. The only restrictions are for very ductile materials and extremely sensitive surfaces.

Set-up: The mechanical components of the Target Scanner are shown in Figure 1. The whole set-up is mounted on a vibration-



Figure 1: Set-up of the Target-Scanner

damped table from NEWPORT that guaranties a stable horizontal positioning of the table top. The positioning unit consists of two linear positioning stages from Schneeberger with a maximum travel of 300mm and 600mm respectively that are mounted perpendicular to each other and are driven by a 2-axes servo motor controller. At the front end of the upper stage the samples can be mounted with different self-constructed sample holders and can be moved relatively to the fixed thickness measuring unit. This thickness measuring unit consists of two digital length gauges from Heidenhain mounted in vertical position in such a way that the difference of the two

length signals gives the thickness of the sample at the respective point, as one can see in Figure 1. Each length gauge has a travel of 60mm in maximum and an accuracy of $\pm 0.1\mu\text{m}$.

Software: LabVIEW was a good candidate for GSI to support developments of small and medium sized control systems and test stands. This project seemed to be a good choice to evaluate LabVIEW. We could make use of the Graphical user interface, the 3D graphics, the advanced analysis, the SQL-Toolkit, the Internet-Toolkit, the VISA interface, the NI hardware, and guidelines of instrument driver developments.

Because no LabVIEW instrument drivers were available for ND231 and SM300 they were developed at GSI. Both instrument driver libraries were developed with respect to the NI recommendations. High level VI's are provided to access all parameters described in the manuals. The details of the communication protocol are not seen by the user.

All data, configuration, measurement and analysis data are stored in a relational database (Oracle). The database design is shown in figure 2. The data is required for experiment analysis. Oracle security is used to control access by the LabVIEW application before any movable devices are initialized.

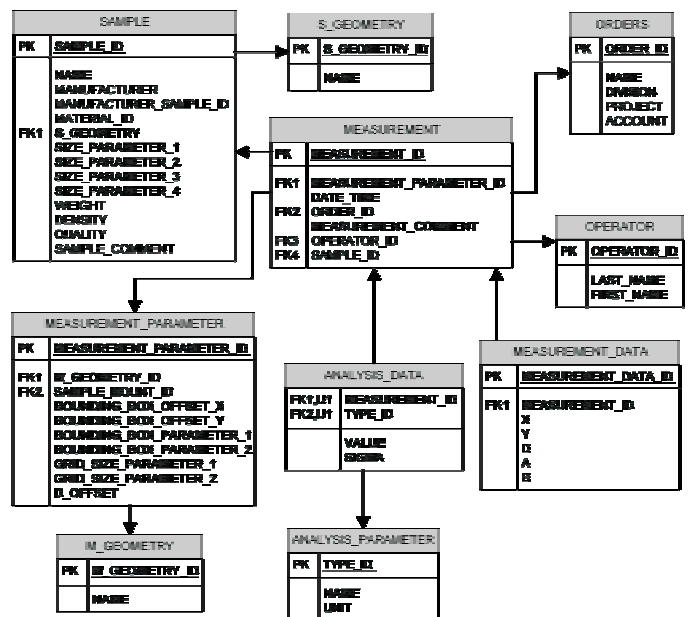


Figure 2: Oracle Database Design

Status: The mechanical components as well as the controlling components and software are ready and tested. The resolution of the thickness measurement is better than half a micrometer and the accuracy of the positioning is $\pm 2\mu\text{m}$, as expected. During the first measurements we found some critical points that could influence the results considerably, for instance, the exact mounting of the sample, the time-dependent deformation of the soft measuring tips and films or dirt on the surfaces of the sample or tips. These errors have to be eliminated or, at least, have to be taken in account. After the last debugging run in the next step the comfort in software handling will be proved and an automatic report and data evaluation will be implemented.

Improvement of the Target Durability for the Heavy Element Production

S. Antalic, H.-G. Burkhard, P. Cagarda, D. Gembalies-Datz, W. Hartmann, B. Kindler, J. Klemm, J. Kojouharova, B. Lommel, R. Mann, H.-J. Schött, J. Steiner, D. Ackermann, F.-P. Heßberger, S. Hofmann

Introduction

The search for new elements with low production cross sections makes it necessary to enhance the beam intensity on the target in order to keep the required beam time at a reasonable length. For element 112 for example the cross section for the synthesis was ~ 1 pb. This corresponds to one event per week on average [1]. A higher beam current, however, leads to severe problems concerning the targets. To synthesize heavy elements at the SHIP set-up lead and bismuth targets are used [2]. At present the maximum beam intensity is limited by the low melting temperatures of lead with 600 K and bismuth with 544 K, respectively. In this range the cooling via radiation is small. Since the target wheel rotates in vacuum there is also no heat conduction via surrounding gas. The third mechanism for temperature reduction is heat conduction along the target itself. But since the target layers are very thin and the amorphous carbon layers are poor thermal conductors, this process is not very effective. Therefore, technical improvements had to be developed in order to protect the targets from melting.

Implemented Improvements:

Several improvements to reduce the stress on the targets are already implemented [3]. After an increase of the active target area by nearly 60%, the Gaussian-like intensity profile of the heavy-ion beam was refined to illuminate the area as complete as possible. To optimise the intensity distribution, two octupole magnets will be installed in the beam line, allowing for a rectangular beam intensity profile across the size of the beam spot.

The background of scattered particles at the detector position has higher energies on the left hand side than on the right. A reduction of this background with a homogeneous degrader is not very effective since one has to take care not to absorb the reaction products. We therefore developed aluminium degraders with a wedge-shaped thickness profile. Depending on the projectile-target combination, degraders with a slope of up to 3 μm over 100 mm length are used. This results in a reasonable compromise between background reduction and slowing down of the evaporation residues, since too low kinetic energies of the latter lead to too low implantation depths and thus to losses of escaping alphas.

To further enhance the durability of the targets at high currents, we investigated different possibilities in parallel that could possibly be combined later on, as there are chemical compound targets, target cooling, and target monitoring [4].

Chemical Compound Targets

The first idea concerning the improvements for the target material itself was to find some chemical compound of lead and bismuth, which is suitable and has a higher melting temperature compared to that of the pure element. We decided to concentrate in the beginning on lead compounds since this is the target material that is needed more often. There exist significantly more binary phases for lead than for bismuth; with

the help of the known phase diagrams and suitable vapour pressures several compounds are ruled out.

The compound in question should be non-toxic, the melting temperature being considerably higher than 700 K in order to profit from radiation cooling. On the other hand the evaporation temperature should not be too high because then the target material would have to be evaporated with an electron gun which involves a much higher material consumption than thermal evaporation. For highly enriched material that could be very cost-intensive.

Up to now we have already synthesized and evaporated two lead compounds, namely ^{208}PbS and $\text{Tm}^{208}\text{Pb}_3$. Leadsulfide has a melting temperature of about 1400 K but at approximately 1220 K it already has a vapour pressure of 10^{-3} bar. The evaporated targets look very homogeneous. They have a black colour which should be advantageous concerning the radiation cooling. The targets do not show any signs of aging, oxidation or other visible alterations, and they are mechanically stable. A disadvantage could be that the compound is non-metallic and therefore electrostatic charging could become a problem. With a scanning electron microscope one can see that the surface consists of very small needles and looks furry.

$\text{Tm}^{208}\text{Pb}_3$ is a metallic compound. Since there is no known binary phase diagram, we estimated the melting temperature from two neighbouring phase diagrams of rare earth elements with lead, namely DyPb_3 that has a melting temperature of $T_M \sim 1170$ K and YbPb_3 , $T_M \sim 1010$ K. Presumably the melting temperature of the thulium compound should be somewhere in-between. We chose thulium despite these unknown quantities since thulium is the most insensitive one of the rare earth elements that usually are oxidized easily. The material as evaporated looks a bit brittle but in principle homogeneous and mattly metallic. But this material shows an obvious aging after one or two weeks. There is a sort of whisker growth of metallic lead on the surface. Besides, the surface begins to look inhomogeneous and starts to oxidize after some time.

Targets were produced from both compounds but they could not be tested with the heavy-ion beam so far.

Target Cooling

Another possibility to avoid the melting of the targets is an active cooling with a He-jet. A He-jet will be blown at the beam spot on the target thus transporting heat load away from the target surface. Additionally the He-jet will result in a low pressure He-atmosphere in the target chamber thus allowing for a cooling of the whole target wheel through convection and conduction. In order to avoid vacuum windows, the whole target chamber of SHIP will have to be reconstructed a differential pumping system has to be installed. To optimise the measures and distances for this new target chamber design, test experiments are inevitable.

Target Monitoring

Another item, we are working on, is a new target monitoring

system. On the one side we use an infrared camera to observe the thermal distribution across the target during irradiation. It is also helpful for the controlling of the experiments concerning new target materials and target cooling. On the other side we work on the implementation of an online thickness measurement of the targets by scanning them with an electron beam and analysing the energy loss behind the target with a position sensitive detector. This will be done in a position of the wheel opposite to the irradiation spot.

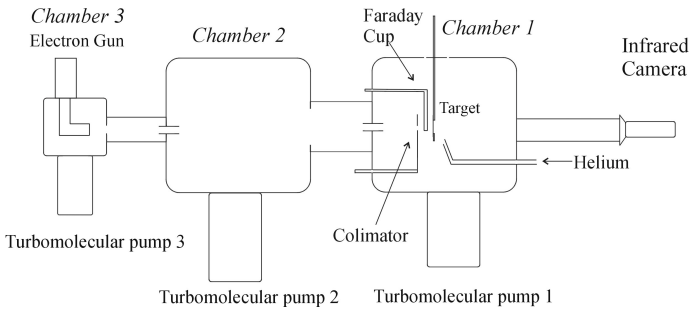


Figure 1: Test bench for high-current production target at SHIP. The target in Chamber 1 is heated by an electron beam. The electron beam can be measured by a movable Faraday cup. The target can be cooled with a He-jet guided through a Laval nozzle. The temperature distribution is measured via an infrared camera.

Test Bench for a high-current Production Target

Since beam time is rare, valuable and the most expensive part of heavy-ion experiments we had to create the possibility to test offline all the improvements described above. We therefore constructed a set-up where all the components developed can be built in to test and optimise the dimensions and the overall performance.

The test bench basically consists of three vacuum chambers arranged in a line, as is shown in Figure 1. Each chamber is connected with a high vacuum pumping system with turbomolecular pumps. The heavy-ion beam is simulated by an electron beam. The electron beam gun is mounted in chamber 3 and the electron beam is guided and focused by electromagnetic lenses on the target, which is placed in chamber 1. Behind chamber 1 an infrared camera is flanged to a long tube so that the target can be observed from the rear side. The temperature distribution of the beam spot on the target as well as melting of the target material can be recorded. By holding the power of the electron beam constant the durability of up to five different target materials mounted on one ladder can be compared directly with each other. Also depicted in Figure 1 is the first stage of the target cooling with a He-jet which is transported directly to the electron beam spot on the target via a Laval nozzle.

Recently the fixed target ladder was replaced by a target wheel that can be driven in the same way as in the SHIP set-up. In Figure 2 two infrared snapshots of a target mounted on a target wheel in the test bench are shown. In both cases the target wheel was rotating with 375 rpm. In the upper picture the wheel was rotating in vacuum and an energy of 1.3 W was deposited in the target with the electron beam. In the lower picture the chamber was filled with a low pressure atmosphere of 0.6 mbar He. To reach the same maximum temperature of 150°C as in vacuum an energy deposition of 2.7 W is needed.

The energy increase of 1.4 W is a measure for the cooling efficiency of the additional atmosphere. In the same way the cooling efficiency of the He-jet or He-jets, blowing from both sides onto the target, will be tested and optimised. It is also noteworthy that minimum temperature of 85°C in vacuum (upper picture) is reduced to 35°C in He-atmosphere (lower picture).

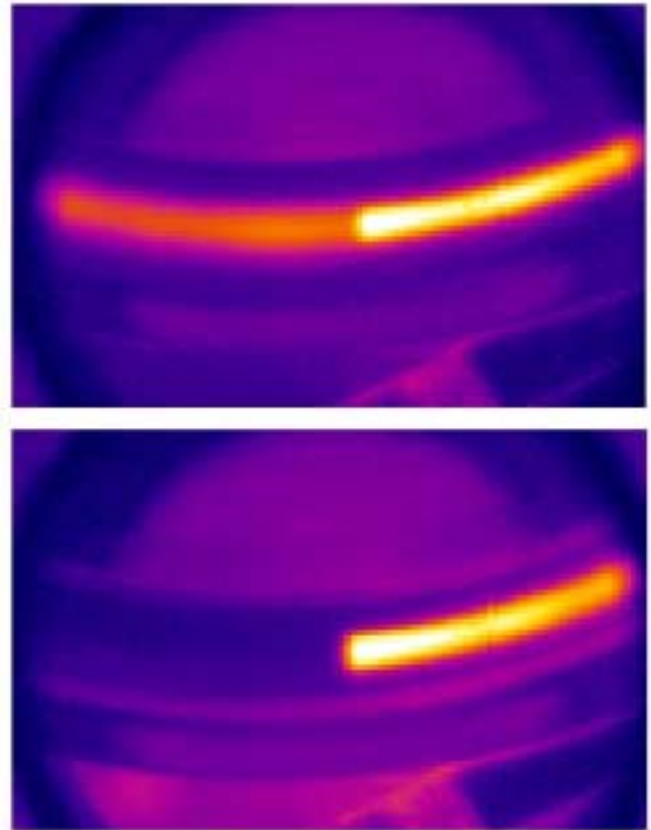


Figure 2: Infrared snapshot of ^{208}Pb -targets mounted on a wheel rotating counter clockwise with 375 rpm. *Upper:* In vacuum, deposited energy 1.3 W; *Lower:* In 0.6 mbar He-atmosphere, deposited energy 2.7 W.

The test bench is also applied for the development and testing of the differential pumping system. Further on the online thickness monitor will be implemented in the test bench with a second smaller electron gun mounted in front of chamber 1.

We also try to reproduce the measured data by temperature calculations. These calculations are performed as function of the velocity of the target wheel, the backing material and backing thickness, the gas flow and the geometry of the target cooling.

References:

- [1] S Hofmann. and G. Münzenberg., *Rev. Mod. Phys.* **72**, 733–767 (2000).
- [2] H. Folger et al., *Nucl. Instr. and Meth. A* 362, 64-69 (1995).
- [3] B. Lommel et al., to be published in *Nucl. Instr. and Meth. A*
- [4] B. Kindler et al., to be publ. in April 2001 in the *Proceedings of the 16th International Conference on the Application of Accelerators in Research and Industry*

Strong Pulsed Magnetic Quadrupole Lens

V. Chichkine¹, M. Winkler³, K.-H. Behr², H. Geissel², A. Kalimov¹, G. Li³,
G. Muenzenberg², C. Scheidenberger², H. Weick², H. Wollnik³

¹St-Petersburg Technical University, Russia

²GSI Darmstadt

³2. Physikalisches Institut, Universität Giessen

In a recent test experiment we could successfully focus for the first time a high-energy heavy ion beam at the FRS using a high-current pulsed quadrupole lens. Such a lens, most frequently used in accelerator technology, can be built by arranging four electric conductors parallel to the optic axis. Pulsing a strong electric current through neighbouring conductors in opposite directions will produce a magnetic field distribution of fourfold symmetry.

The overall length of the used quadrupole lens was 97 mm with an aperture diameter of 20 mm. The pulse generator consisted of a capacitor bank of 1640 μF with a maximal charging voltage of 3.2 kV which corresponds to a stored electric energy of 8.4 kJ. The pulse period of the current oscillation was $\approx 500 \mu\text{s}$ [1]. The electric current was controlled by a power thyristor with a maximal current rating of 34 kA. In this case the achievable magnetic field gradient in the quadrupole is more than 1000 T/m [2].

In the experiment the FRS was mainly used as a transport system. The pulsed quadrupole was placed approximately 2 m behind the final triplet of the FRS. Another 300 mm downstream from the pulsed quadrupole a scintillator target was set and the beam profile was monitored by a CCD camera (Fig.1).

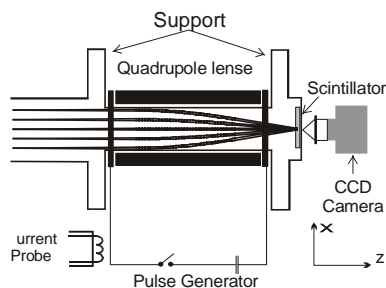


Fig. 1. Experimental setup to focus an initially parallel high-energy heavy ion beam with a pulsed quadrupole.

In the experiment a $^{197}\text{Au}^{79+}$ heavy ion beam was used with an energy of 650 MeV/amu which corresponds to a magnetic rigidity of the beam of about 10.5 Tm. The final quadrupole triplet of the FRS provided a parallel beam at the entrance of the pulsed quadrupole. The SIS was operated in the fast-extraction mode where 4 bunches per spill are extracted in $\approx 1 \mu\text{s}$. Since the flat-top of the current oscillation is about 10 μs a quasi constant magnetic field is put up during the beam extraction. To determine the focusing properties of the quadrupole the pulse generator was charged stepwise from 0 to ≈ 2.5 kA and for each step the resulting beam

profile on the scintillator screen was measured. The smallest beam size was observed at a charging voltage of 1.4 kV. This corresponds to a peak current of about ≈ 11 kA and a magnetic flux density of ≈ 4.65 T respectively at the surface of the quadrupole wires. The beam, which was initially ± 10 mm, was focused to approximately ± 2.5 mm which is limited by the emittance of the beam. Applying higher charging voltages led to a defocusing of the beam.

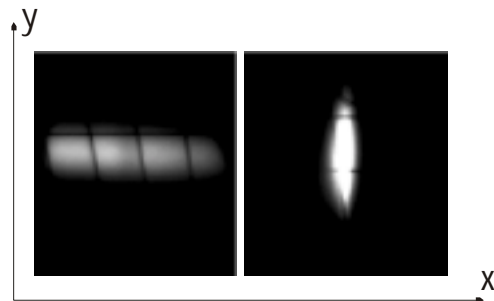


Fig.2. CCD snapshots: a beam with an initial size of ± 10 mm (left) could be focused to ± 2.5 mm (right). The grid size is 5 mm .

One of the feasible applications for pulsed quadrupole lenses is a short focal length condenser system (Fig.3.), with which it's possible to increase the transmission for nuclear reactions products [3]. Such condenser lenses must be arranged shortly behind a reaction target and have a focal lengths as short as possible. Corresponding quadrupole lenses thus should have small apertures and high field gradients. One such condenser system has been designed for the projectile fragment separator at GSI, Darmstadt [4].

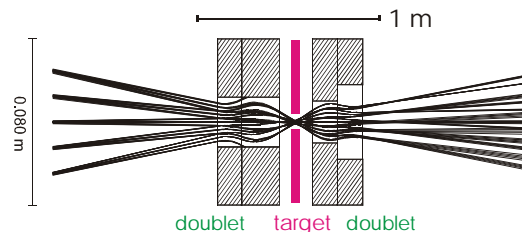


Fig. 3. A condenser system as a possible application for strong focusing lenses.

References

- [1] G. Li et al., Rev. Science. Inst. 71 (2000) 376.
- [2] V. Chichkine et al. NDTCS-2000, Vol 4, A 6.
- [3] H. Wollnik, Nucl. Instr. And Meth. Vol 83, (1970), 229.
- [4] H. Geissel et al., GSI Report 89, 30, (1989).

CVD-Diamond Detectors - Status Report 2000

E. Berdermann, H. W. Daues, P. Moritz, H. Stelzer, B. Voss

The excellent results obtained from CVD-diamond detectors in heavy-ion timing measurements with intense beams initiate applications in new fields [1]. A large area (6 x 4 cm²) diamond strip detector of 200 μm thickness containing 32 strips of a 1.8 mm pitch has been successfully used in the atomic physics Cave A at GSI as the focal plane detector of a magnetic spectrometer. Beam loss monitors are under consideration, enabling controlled beam transport in hot regions along the high-current injector beamlines. Very first results from the time resolution in measurements with minimum ionizing particles are encouraging. Polished CVD-diamond material with a collection distance > 200 μm is being used for. Because of the much better Signal-to-Noise ratio required, new timing amplifiers are currently under development [2].

The investigations of CVD-diamond detectors are continued with studies of the influence of the electric field and the bias polarity to the detector response. A variety of papers [3] is available in the literature discussing the origin and the nature of numerous trap levels detected in the range from 20 meV to 3.6 eV in CVD diamond. Due to the appearance of fixed space charge in the diamond bulk, the electric field inside the detector is not homogeneous. The mobility of carriers in the crystalline grains is orders of magnitude higher than in disordered grain boundaries. Conductivity models are discussed, where the average collected charge is affected by electron capture in grain boundaries (assumed as amorphous carbon) and hole capture in grain defects. Because of the columnar growth structure of the polycrystalline CVD diamond the electrical behaviour of material neighbouring nucleation side is quite different compared to the growth side. The influence of the detector thickness to this picture is obvious.

Three detectors made of unpolished CVD diamond grown with identical process parameters but different thicknesses were used to study the detector behaviour under different electric field conditions. The detectors of an 1 cm² area were mounted in a stack with increasing thickness in beam direction ($d_{D1} = 93 \mu\text{m}$, $d_{D2} = 158 \mu\text{m}$, $d_{D3} = 246 \mu\text{m}$). The beam test has been performed with ⁸⁴Kr projectiles of 650 MeV/amu.

The data obtained are limited by the bandwidth and the sensitivity of the available electronics. In order to avoid saturation of the pulse heights as observed for D2 and D3 in some cases (see Fig. 2, Fig. 3) a new amplifier DBAIII (3 GHz) with variable gain 1:100 has been developed. Low sensitivity QDC's and TDC's of higher resolution than the currently used (25 ps/ch) are urgently required for future measurements.

Characterisation data of the D1 sample ($d = 93 \mu\text{m}$, $C = 37 \text{ pF}$) are shown in Fig.1. The pulses (a) demonstrate the limitation of

the measurement system to determine the signal rise time. Commonly, a higher amount of charge is collected for positive bias on the growth side whereas a shorter carrier drifttime is observed for negative polarity (b).

Fig.2 shows the timing results obtained from each diamond detector versus a plastic scintillator used in coincidence. The σ -widths of the ToF spectra are plotted over the electric field applied in (a) and over the detector thickness in (b).

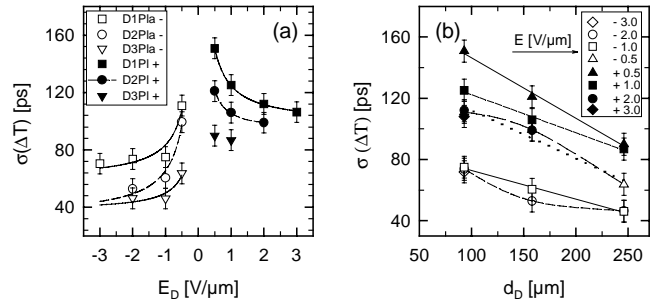


Fig. 2: ToF resolution measured with three diamond detectors of different thicknesses versus a scintillator detector. The σ -widths of the ToF spectra are plotted over the applied electric field E in (a) and over the detector thickness in (b).

The corresponding pulse-height results are shown in Fig. 3.

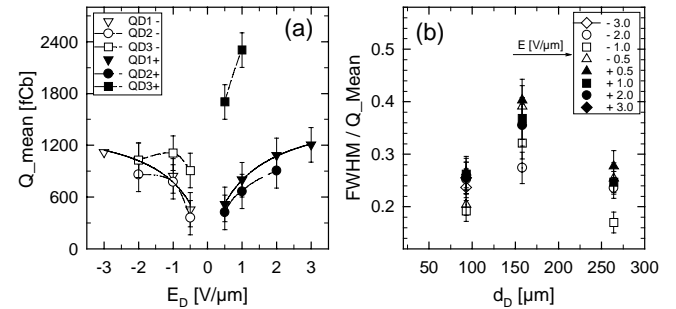


Fig. 3: The mean collected charge plotted over the applied electric field (a) and the pulse-height resolution under the same electric field conditions over the detector thickness (b).

Due to saturation effects of the D2 and D3 pulse heights no final conclusions concerning the thickness dependence of the collected charge signal can be extracted quantitatively. Nevertheless, the general trend is obvious. For both polarities the data indicate an erratic increase of the collected charge above a certain thickness. Although the charge collected with positive bias on the growth side is much higher, the best time resolution is obtained for thicker detectors at the highest negative electric field. These data have to be confirmed.

References

- [1] E. Berdermann et al., "The Use of CVD Diamond for Heavy-Ion Detection", 7th Int. Conf. on New Diamond Science and Technology, Hong Kong 2000, to be publ. in Diamond and Related Materials (2001)
- [2] M. Petrovici et al., "Preliminary Results on Timing Properties of CVD diamond Detectors for MIPs", GSI Internal Report 2000
- [3] Diamond Data Base, "http://www.tribology.dti.dk/cgi-bin/DIA_database"

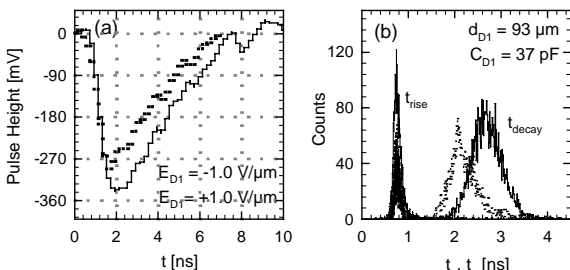


Fig 1: (a) Single-particle pulses at positive resp. negative bias. (b) The corresponding rise-time and decay-time distribution

FOPI Trigger: Improving Statistics on Strange Particles

O. Brosch, A. Kugel, R. Männer – Lehrstuhl für Informatik V,
 Universität Mannheim, Germany (brosch@ti.uni-mannheim.de)

Introduction. FOPI experiments produce low statistics with respect to certain strange particles, especially negatively charged kaons [1]. The reasons are their rareness and the slow data read-out even with the updated FADC scanning system [2]. Thus, a trigger system is required to ensure that only events containing these particles are read by the FADC scanners [3]. We have investigated, how our trigger algorithm [4] can increase strange particle yield and how this affects hardware [5] requirements.

Trigger Concept. The trigger will be integrated into the experiment as follows: the central drift chamber's (CDC) sense wires signal is passed to the trigger via a discriminator, circumventing the FADCs. The trigger algorithm extracts the particles' track information, and together with the time-of-flight data determines the particles' species. If an anti-kaon is found the FADC scanners get a "start read-out" signal. If not, read-out time is saved.

Performance. The first version of the trigger algorithm [4] was designed to classify – under optimal conditions – every particle contained in the CDC data. While this is the best way to analyze a single event, the procedure does not significantly increase the number of kaons that can be recorded during an experiment of fixed duration.

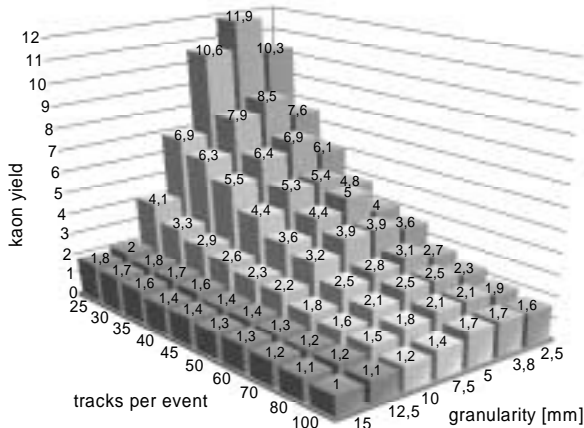


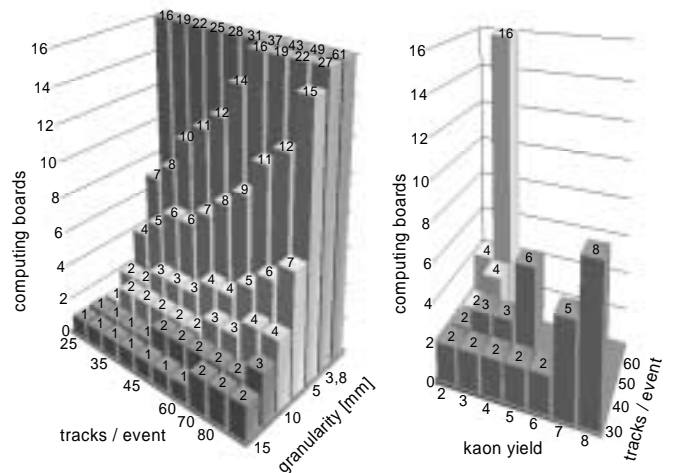
Fig. 1: kaon yield vs. granularity and occupancy.

Ghost Tracks. A simulation was elaborated that produces the number of kaons that can be found in a given period of time rather than the percentage of particle tracks that can be classified accurately. The result is that the number of detected kaons highly depends on the number of "ghost tracks" and only secondarily on the percentage of accurately classified particles. The number of ghost tracks in turn basically depends on the occupancy in the detector image, i.e. the number of particle tracks contained in the sense wires' signals. Ghost tracks emerge from sets of hits that incidentally form a track. Their number is significantly increased by the fact that – induced by the CDC design – 50 percent of the detector's signal lead to mirrored hits. To focus on suppressing ghost tracks turned out to be the proper strategy for increasing the yield of a certain

particle species. Other parameters, like granularity of search patterns or filter operators, were used to fine-tune algorithm performance. Another interesting result is that kaon yield does not significantly depend on the algorithm's execution time.

Kaon Yield. Compared to kaon yield without a trigger our simulation suggests that the algorithm can increase the number of kaons by a factor of ~3 with approximately 50 particle tracks per event, and a factor of ~6 to 8, if only ~30 particle tracks occupy the detectors' data. Fig. 1 shows the dependence of the yield as a function of occupancy (number of tracks) and granularity (resolution of predefined tracks or number of search patterns).

Hardware Requirements. Hardware consumption of the FOPI trigger algorithm primarily depends on the granularity, i.e. how many predefined patterns have to be compared with the hits on the CDC wires (the detector image). A second important parameter is the occupancy and the size of the hit space, i.e. the number of tracks, detector pixels per track and thus of active pixels in the CDC. The latter determines the algorithm's execution speed. Fig. 2 shows hardware consumption as a function of granularity, occupancy, and kaon yield.



The New Readout Electronics for TAPS*

P.Drexler², U.Thöring², W.Bonn², H.A.P.van der Duin³, R.Holzmann¹, G.van der Kruk³, B.Krusche⁴,
H.Löhner³, V.Metag², T.W.Nijboer³, J.G.Messchendorp², R.Novotny², C.Salz²,
S.Schadmand², M.Steinacher⁴, M.Thiel², H.Vorenholt³, *for the TAPS collaboration*

¹ GSI, Darmstadt

² II. Physikalisches Institut, Universität Gießen

³ KVI, Groningen, The Netherlands

⁴ Department of Physics and Astronomy, University of Basel, Switzerland

The new readout electronics for the electromagnetic calorimeter TAPS is being built by the Gießen physics department in collaboration with KVI, Groningen (The Netherlands) and the University of Basel. It is planned to employ the new electronics in joint experiments with TAPS and the dilepton spectrometer HADES at GSI, Darmstadt. The concept is based on the VME-standard and accommodates modern expectations regarding data rate, resolution, flexibility and trigger selectivity. An additional requirement is compatibility with the HADES readout system [1].

An 8-channel prototype miniseries from the new VME-readout electronics for the electromagnetic calorimeter TAPS [2] has been employed during a first test beam time at the MAMI tagged photon beam facility. The analog functions for the TAPS telescopes (BaF₂ scintillators and TAPS Veto System) are implemented on a piggyback residing on HADES/TAPS ADC Motherboards [3]. The determination of time-of-flight information (time chain) as well as the separate charge integration of the two scintillator components with two dynamic ranges (energy chain) has been implemented for each BaF₂ detector. The piggyback board logic is derived from constant fraction discriminators. Additional leading edge discriminators allow fast, selective triggers. Programmable logic devices (PLD) are used bi-directionally for setting discriminator thresholds and, during data taking, for registering the discriminator signals. A prototype for a 64-channel multiplicity coincidence unit for the TAPS first level trigger has been completed and tested. Test results of the time chain using a time calibrator have been reported earlier [2].

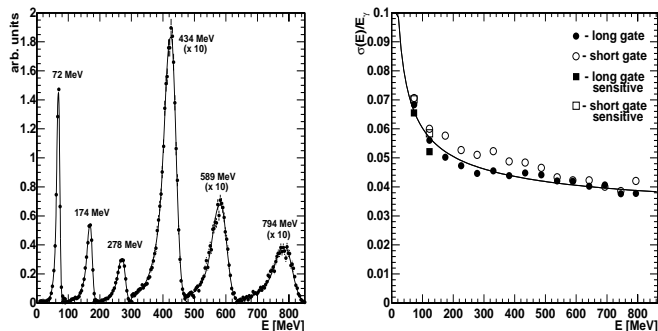


Figure 1: *Left: Shower line shapes for various incident photon energies from the first in-beam test measurement with 7 BaF₂ crystals. Right: Energy resolutions for the 4 integration gates as a function of incident photon energy.*

An in-beam test was performed to study the energy resolution and linearity. A detector array consisting of 7 BaF₂-crystals was placed in the tagged photon beam. Figure 1 presents the energy response to incident photon energies between 70 and 800 MeV. The analog signals have been integrated over 2μs with a full scale range of 1 GeV. The line shapes are fitted with the typical response of BaF₂ crystal arrays (solid lines). The corresponding resolutions (σ) as function of incident photon energy are also shown in Figure 1.

A second test measurement employing a mini-series of the new TAPS electronics is realized by participation in a current TAPS experiment at MAMI. The experimental setup includes the TAPS detector in a wall formation placed on one side of the beam covering ca. 30% of 4π. The small detector array (7 BaF₂ crystals) is placed on the other beam side at 100° and read out by a HADES-compatible acquisition. Figure 2 presents the π⁰ → γγ invariant mass peak from the reaction γ + ⁴He where one of the final state photons was detected in the small detector array read out by the new electronics. The figure demon-

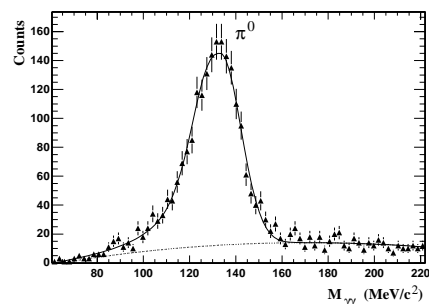


Figure 2: *The π⁰ → γγ invariant mass peak from the reaction γ + ⁴He. One of the final state photons was detected in the small detector array read out by the new TAPS electronics prototypes. The solid line represents a fit with the known π⁰ → γγ line shape plus background (dotted line).*

strates the clean observation of γγ invariant masses, being one of the key ingredients of a standard TAPS analysis.

Milestones for the year 2001 include the final revision and mass production of the TAPS piggybacks. The readout of four channels per VME module is foreseen to be managed per motherboard. Accordingly, the BaF₂ calorimeter with a planned total of 9x64 detectors necessitates 144 VME-modules.

* supported by BMBF, GSI, SNF, and FOM

References

- [1] <http://www.physik.uni-giessen.de/hades/>
- [2] GSI Scientific Report 1999
- [3] R.Bassini et al., A 32 Channel TDC on a VME-Board, IEEE Trans. on Nucl. Science, Vol. 45, 3, June 1998

New data acquisition system for CERES/NA45 at CERN

P. Braun-Munzinger, J. Holeczek, D. Miśkowiec, H. Sako, GSI
H. Tilsner, H. Wessels, University of Heidelberg

For the 2000 run of CERES a new TPC readout scheme was implemented [1]. The data acquisition system (DAQ) needed to be adapted to the new readout. Between March and September 2000 we designed and implemented a completely new DAQ. It was then successfully used to collect 30 millions central Pb+Au events in the 160 GeV/nucleon run. Below we briefly describe the DAQ scheme and performance. More details can be found in [2].

The new DAQ was to a large extent based on standard hardware components (20 personal computers under linux) and software tools. It was highly modular so we could optimize one part of the system without touching the others. Ten readout PCs were collecting events during the 5 s long SPS burst. In the 14 s long burst pause they were sending the collected data via ethernet to an event builder PC in the CERN Central Data Recording facility (CDR). There the ten data buffers were merged into one and saved on disk. The tape daemon, asynchronously running on this machine, copied the file to tape. The cleaner process was deleting the oldest files such that half of the disk space was always available. Below we go through the collecting, storing, sending, and event building stages in more detail.

Charges induced on the TPC readout pads were digitized in FEDC modules [3] sitting in VME crates in the experimental zone. Each VME crate was connected via a MXI interface and a 20 m cable to a readout PC, located in the counting room. Eight readout PCs were needed to read the 16 TPC chambers. Other CERES detectors, SDD, RICH1, and RICH2, sent their data via receivers to memory modules, then via optical links and O2PCI modules to the memory of an embedded PC. The beam detectors ADCs and TDCs in three daisy-chained VME crates were accessed by yet another readout PC via PVIC.

The readout was triggered by an external signal applied to an input channel of an I/O card (PC36C by Eagle Technology) plugged in each readout PC. The collector software was polling on the bit. Once a trigger has been seen, the PC would set a busy signal on an output line of the I/O card. A logic OR of all busy signals went to the trigger system and inhibited new triggers. The busy signal was removed only after the complete data had been in the memory of the PC (unless in the pipeline mode, see below).

The event size was 0.5 MB. The average busy duration, i.e. the average time needed to get the event into the memory of a readout PC, was 1.7 ms for the beam detector crates, 3.8 ms for SDD, 2.3 ms for RICH, and 5.7 ms for TPC. The largest fraction of the latter was spent in the data transfer from the FEDC to the readout PC via MXI (12 MB/s). With the beam intensity of 10^6 per burst, and with the centrality trigger of 8%, the rates of offered and accepted triggers per burst were 1000 and 300, respectively. In the middle of the run a pipeline readout was implemented for the TPC. The 5.7 ms were split in two parts: ~ 1 ms,

needed for the data to get in the ALTRO chips of the FEDC, and ~ 5 ms for the transfer to the readout PC. The number of accepted triggers increased to 400 per burst.

On all readout PCs the data were collected in the upper most 64 MB of the total 128 MB physical memory. This memory was disabled for linux by an appropriate entry in `lilo.conf`. A memory device driver, similar to `mem.c`, was used to access this area via `/dev/daqmem`. From the system level the user could handle `/dev/daqmem` like an ordinary disk file, including dumping, editing, copying, etc.

The collecting was controlled by a set of parameters, residing in the kernel memory. After a trigger, the collector process would read them to know where to store the event. After storing it would update the appropriate numbers. Later, when the burst was finished and the data needed to be sent to CDR, the sending routine would read the parameters to figure out how many bytes to send. The access to the parameters was provided via a simple device driver. From the system level the user could access the parameters at any time via `/proc/daqctrl`.

In the burst pause the readout PCs sent the collected data to one event builder PC in CDR via sockets. The 10 receiver processes, running on the event builder machine, dumped the data into named pipes (FIFOs). The sending speed of each readout PC was limited to about 10 MB/s (fast ethernet). The Gigabit ethernet card on the CDR side, however, was limiting the total transfer rate to 30 MB/s. Furthermore, because of the run control overhead and because of activities on the event builder PCs, only 200-250 MB of burst data could be sent within the burst pause in a stable mode. This was the bottle neck of the DAQ. The resulting continuous data rate was 10 MB/s.

The event builder (evb) read the FIFOs, checked the consistency of event counters, merged the subevents, and saved the output, containing one complete burst, to a disk file. The processing speed was 15-17 MB/s and thus the data of the next burst had to be sent to a different CDR machine. In total seven event builder machines were used.

A tape control script sorted link files created by evb into tape job queues and submitted them on each evb machine. Typically there were 1-3 jobs per machine. The actual copying to tape was done using CERN `tpwrite` with 5 MB/s. The overall taping rate was limited to 20 MB/s.

The new DAQ, in spite of various problems, was working from the beginning of the heavy ion run and allowed to collect total of 30 millions events.

References

- [1] H. Tilsner, GSI Annual report 2000.
- [2] <http://www.gsi.de/misko/ceres/daq/note.html>
- [3] Design by Luciano Musa, CERN.

The New Readout Electronic for the CERES TPC

C. Engster¹, P. Glässel², J. Holeczek², M. Joos¹, D. Miśkowiec³, L. Musa¹, M. Richter²,
H. Sako³, W. Seipp², J. Stachel², G. Thomas¹, H. Tilsner², J. Wessels²

¹ CERN, ² Universität Heidelberg, ³ GSI Darmstadt

For the CERES beam-time in 2000 the readout system of the TPC was completely changed. A modified version of the original front-end board (see fig. 1 and [1]) and the motherboards were still used. The electronics close to the DAQ (receivers, memory modules, Compact PCI system) was replaced by newly designed boards (**F**ront **E**nd **D**igitization **C**ards). The design of these cards is based on a development for the ALICE TPC readout system. In the new setup the motherboards were used for configuring the front-end electronics and for distributing the trigger and abort signals.

Immediately after receiving a trigger signal the SCA (Switched Capacitor Array) on the front-end board starts to sample the 16 outputs of the amplifier in parallel. Up to 250 individual time samples for each channel can be stored to allow three-dimensional reconstruction of the tracks. The sampling phase is followed by the readout phase in which the stored analog values are dumped in a time-wise order. During the readout phase the output signal of the SCA has a maximum swing (AC component) of 2 V and a baseline (DC component) that can be adjusted online via a DAC on the front-end board.

The digitization and further processing of the TPC signals is done on the FEDC-boards. These boards are realized as 9U VXI devices which can contain up to 48 readout channels. Each readout channel comprises a 10-bit ADC and a digital chip for signal processing (a modified version of the ALTRO chip for the ALICE TPC [2]) and processes the data from one front-end board. After converting the analog signal the data stream is demultiplexed according to the 16 channels of the preamplifier. The resulting 16 data streams are processed in parallel inside the ALTRO chip. The data is represented and processed only with the 9 MSB, resulting in a loss of 1 bit in resolution. Therefore, the signal is described by a 9 bit code (0 – 511).

In the following processing steps the polarity of the signal is changed and the baseline is subtracted. After this subtraction the signal should be contained in the first half of the 9 bit range. Therefore the most significant bit can be

omitted reducing the signal representation to 8 bit codes. Finally the signal undergoes zero suppression. Samples with a value smaller than a constant threshold (8 bit) are rejected. When a sample is found to be above the threshold, it is considered as the start of a pulse (cluster) and stored in the central memory of the FEDC.

Inside the FEDC an event is stored in memory as a back-linked structure. Due to reordering of samples between accepted clusters, the timing information is lost during the zero-suppression process. This requires the addition of two additional words – the time-stamp and the cluster-length. The cluster-length corresponds to the total number of samples plus the time-stamp and the cluster-length. The time-stamp gives the (sample-)position of the last sample in the cluster relative to the trigger signal. This cluster structure (sample values + time-stamp + cluster-length) is repeated for each accepted cluster in a specific channel. For each channel up to 250 time samples can be accepted.

Because each ALTRO chip processes data coming from 16 TPC-channels with a maximum of 250 time samples, it was not possible to provide enough memory inside the chips to hold pedestal values for all samples. Instead, a scheme using a look-up table was implemented. The look-up table contains 250 7 bit words. The index (the linenummer) of this table corresponds to the sample number. The entries are the addresses of the data-buffers which contain the pedestal values. This means, 128 pedestal values can be assigned to each channel.

Three FEDC boards are combined in one VME-crate. Each of these boards is connected to 40 front-end cards, i. e. processing the data from 640 TPC pads. In total, 24 FEDC boards are needed to read out the whole TPC. The connection between these crates and the readout PCs (cf. [3] for more details) are realized with National Instruments' MXI-bus. MXI-bus is a general purpose, 32-bit multi-master system bus on a cable. It provides a way of controlling VXI systems using commercially available desktop computers and workstations. In CERES a PCI-VME bridge is used. This configuration consists of a PCI card (plugged in the readout PCs), MXI-2 bus and a MXI-VME interface card which is plugged into the VME-crate for the FEDC cards. Data and control signals are converted on the PCI board and sent over the MXI bus, which is essentially the VME on a cable, into the MXI-VME interface board. The 6U MXI-VME interface board in conjunction with the MXI-2 cable enables data transfers up to 38 MBytes/s using D64 transfers.

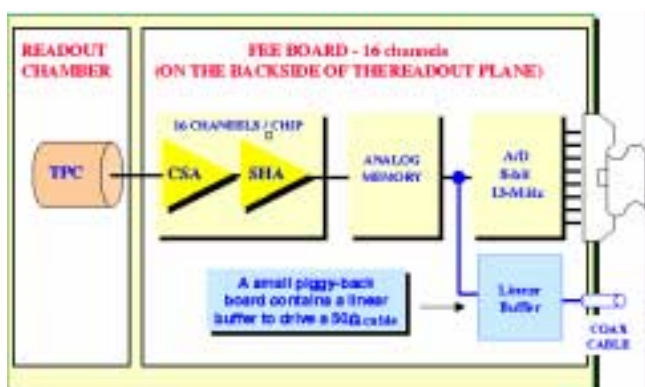


Figure 1: The modified FEE card.

References

- [1] R. Baur *et al.*, GSI Scientific Report 1998 p. 190.
- [2] ALICE Collaboration, Technical Design Report, CERN/LHCC 2000-001
- [3] D. Miśkowiec *et al.*, this Report

Front-end electronics for ALICE TPC-Detector

H. K. Soltveit and J. Stachel

The front-end electronics for the ALICE TPC to read out the charge detected by 570132 pads located on the readout chamber end-caps is here presented. The read-out chambers are multiwire proportional chambers with cathode pad read-out. The pads receive as the image charge of the signal on the anode amplification wires a signal with a fast rise time (less than 1 ns), and a long tail due to the motion of the positive ions. The signal is delivered on the detector impedance which varies between 3 pF to 12 pF. Therefore the front-end electronics must cope with different pad capacities. The electronics will be located in an area with limited access. High reliability is thus a concern. The circuit was developed in 0.35 μm CMOS technology.

The front-end electronics consist of a charge sensitive preamplifier/shaper, a 10-bit 10 MHz low-power ADC and an ASIC which contains a shortening digital filter for the tail cancellation, the baseline subtraction and zero-suppression circuits, and a multiple-event buffer [3]. The image charge induced on the TPC pads is amplified and integrated by a low input-impedance amplifier. It is based on a continuously sensitive charge sensitive amplifier followed by a semi-gaussian pulse shaper of second order. The amplitude, which is different for the 3 different pad sizes, has a typical value of $7\mu\text{A}$.

The Preamplifier/shaper for the ALICE TPC (Fig.1) is based on the design of the preamplifier/shaper for the NA45/CERES TPC. The main modifications concern:

- migration from the technology AMS CMOS 0.8 μm to the AMS CMOS 0.35 μm ;
- optimization of the design to better fulfil the ALICE requirements;
- removal of the tail cancellation circuit that, in the ALICE design, is implemented in the digital ASIC.

This continuously sensitive design is particularly suitable for a detector with high occupancy. A peaking time of $\tau_s = 120$ ns and noise consideration (< 1000 electrons) dictate a P-channel input transistor and a feedback resistance $R_F > 10$ M Ω . The feedback resistance R_F is realized by using a MOS transistor biased in subthreshold region. The MOS transistor MF establishes the DC path and continuously discharges C_F with a decay time $T_{decay} = C_F \times R_{ds}(MF)$.

The only practical way to realize such a high resistance in CMOS technology is by using the associated drain-source $R_{ds}(MF)$ of a MOSFET transistor. A transistor operating in this area is very sensitive to process, temperature and supply voltage variations. To prevent or reduce these effects a Self-Adaptive scheme to bias the feedback transistor MF is used. The MOS-transistor Mzero is

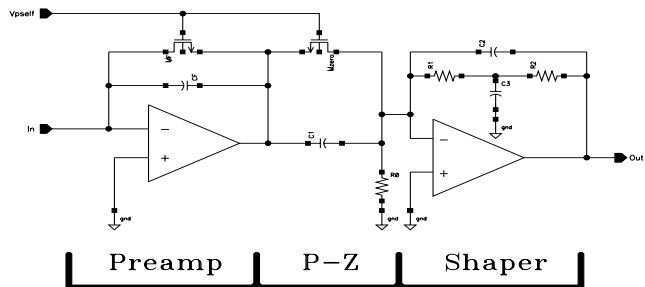


Figure 1: Schematic of the preamplifier/shaper chain.

biased the same way as MF during the discharge of C_F . The Zero associated to the network Mzero-C1, adapts itself dynamically to accurately cancel the pole associated to the network CF-MF. There is also a benefit from the reduction of $R_{ds}(MF)$ at high Q_{in} , i.e. faster return to the baseline of the output of the CSA-shaper, without worsening the linearity of its conversion gain. In terms of noise requirements, the ALICE preamplifier/shaper fulfills the requirement with an ENC of less than 500 electrons for input capacitances between 3 pF and 17 pF. The response is linear ($< 0.2\%$) up to an dynamic range of 1.3 V with a peaking time around 120 ns. The gain of the preamplifier/shaper is about 7.8mV/fC. The total power consumption is 7 mW/channel.

The front-end electronics for the read-out for the TPC has been designed and fabricated with the AMS 0.35 μm CMOS process. The first prototyp is received and a first testing shows promising results. A new version is under development. The main change is the inclusion of a fourth-order filter to obtain a more symmetrical response to increase the double track resolution. The gain of the circuit will also be distributed towards the input to decrease the noise even further.

References

- [1] R.Baur. GSI Annual Report 1997.
- [2] G.Gramegna, P. O'Connor, P. Rehak, S.Hart, Nucl. Instr. and Meth., **A390 (1997)**, 241-250.
- [3] ALICE Technical Design Report, Cern/LHCC, January 2000.

ALICE TPC Readout Chambers

P. Braun-Munzinger¹, J. Fiess², M. Ivanov¹, R. Renfordt², H. Sann¹,
H.R. Schmidt¹, H. Stelzer¹, D. Vranic¹

¹GSI Darmstadt, ²University of Frankfurt

A major component of the CERN-LHC ALICE detector is the central barrel, contained in the large L3 magnet and composed of detectors devoted mainly to the study of hadronic signals [1] and dielectrons [2]. The main tracking devices are the silicon based Inner Tracking System (ITS) and the Time Projection Chamber (TPC). Within their acceptance ($-1 \leq \eta \leq 1$) about 12000 tracks will be recorded, yielding information about particle type and momentum.

The readout planes at the two sides of the TPC field cage are subdivided into 18 segments each. The segments are split into an inner and an outer readout chamber (ROC). The ROCs will be conventional multiwire proportional chambers with cathode pad readout as used in many TPCs before. However, the high particle load puts severe constraints on the design parameters in terms of pad geometry and gas gain and leads to requirements that go beyond an optimization in terms of momentum and dE/dx resolution.

To both minimize the pad occupancy and to ensure a sensible pad response function, $4 \times 7.5mm^2$ pads were chosen for the inner chambers. The outer chambers have a pad size of $6 \times 10mm^2$ (inner half) and $6 \times 15mm^2$ (outer half). Altogether, the inner chamber has 5504 pads, while the outer one has 9984 pads. The wire spacing for both the anode and cathode wires is $2.5mm$, while the gating grid has a wire spacing of $1.25mm$. The distance from the pad plane to the anode wire is 2 and 3 mm for the inner and outer chambers, respectively.

A full size prototype of an inner readout-chamber has been built at GSI in order to verify the design parameters, such as gating efficiency, gas gain, signal-to-noise ratio, pad response function, cross talk, etc.

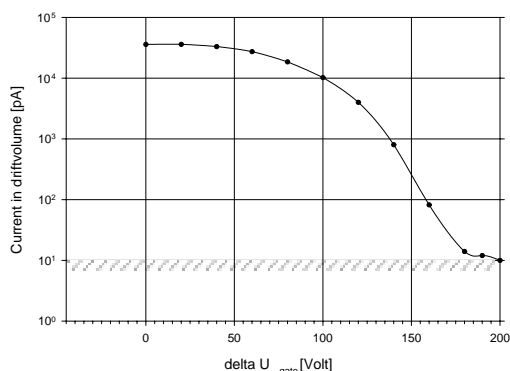


Figure 1: Measurement of ion feedback into the drift volume. The sensitivity limit is indicated by the hatched bar.

The measured gating efficiency against positive ion feedback from the amplification region into the drift region is shown in Fig. 1. The measured current at the drift electrode for gate closed ($\Delta U = 200V$) is $12 \pm 2pA$, which is comparable to the offset current from primary ionization in the drift volume. The total current at the anode

is 115 nA, of which $\approx 30\%$ ($= 34nA$) are seen at the drift electrode. An upper 2σ -limit on the gating inefficiency is 0.5×10^{-4} fulfilling the design requirements.

256 out of 5504 channels have been equipped with CERES preamplifier-shapers. This chip, used in the CERES experiment, is the basis of the ALICE PASA chip and thus comparable in its properties. The RMS noise of the PASA with full capacitive load ($\approx 15pF/pad$) has been measured to be below 1000e, which projects to a signal-to-noise ratio for minimum ionizing tracks better than 20.

The gas gain of the chamber filled with 90% Ne, 10% CO_2 has been determined. The nominal gas gain of 2×10^4 is reached at a voltage of $\approx 1250V$. The chamber, irradiated with a strong ^{90}Sr -source, has been operated stably for several weeks at this gain.

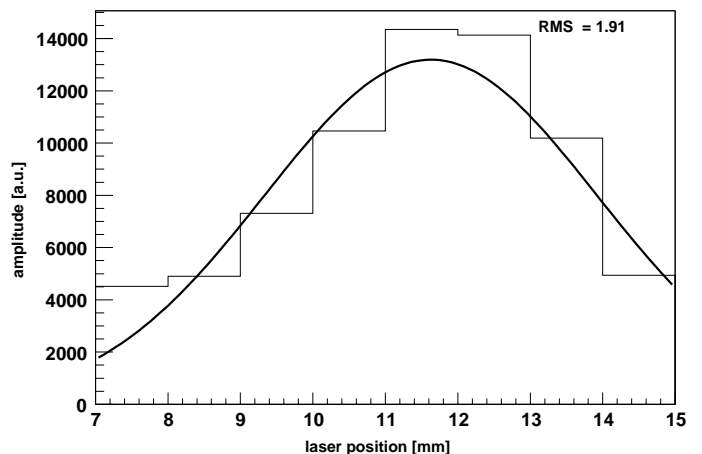


Figure 2: Signal induced by a laser beam.

Fig. 2 shows the response of the chamber to a Nd:YAG laser beam in terms of the pad response function (PRF). The histogram represents the response of a given pad to a laser beam at different positions relative to the pad. From this data the pad response function is extracted to be $\sigma \approx 2mm$ in accordance with the expectations [3]. This number, together with the measured RMS noise figure, allows the conclusion that the prototype chambers work according to the specifications in terms of 2-track and position resolution.

References

- [1] ALICE Collaboration, Technical Proposal, CERN/LHCC/95-71
- [2] ALICE Collaboration, Technical Proposal, Addendum 2, CERN/LHCC/99-13
- [3] ALICE Collaboration, Technical Design Report, CERN/LHCC/00-001

Prototype tests for the ALICE TRD

A. Andronic¹, H. Appelshäuser², C. Blume¹, P. Braun-Munzinger¹, D. Bucher³, G. Cătănescu⁴, M. Ciobanu⁴, H. Daues¹, A. Devismes¹, Ch. Finck¹, N. Herrmann², T. Lister³, T. Mahmoud², T. Peitzmann³, M. Petrovici⁴, K. Reygers³, R. Santo³, R. Schicker², S. Sedykh¹, R.S. Simon¹, J. Stachel², H. Stelzer¹, J. Wessels², O. Winkelmann³, B. Windelband², C. Xu² (ALICE Collab.)
¹GSI Darmstadt, ²Universität Heidelberg, ³Universität Münster, ⁴NIPNE Bucharest

The ALICE Transition Radiation Detector (TRD) has been designed to improve the pion rejection capability of the ALICE detector by at least a factor of 100 for momenta above 2 GeV/c [1]. To demonstrate that this goal is achievable, during the last year we have conducted prototype tests at the pion (with natural electron content) beam facility at GSI Darmstadt. A complete description of the experimental setup and of the results (including references) can be found in [2]. Many types of radiators were tested, composed of foils, fibres and foams. Here we summarize the results concerning the pion rejection performance in case of a fibres (of 17 μm diameter) radiator, which was established to be the best candidate for the final radiator.

The measured distributions of energy deposit over the depth of a drift chamber have been employed as probability distributions in simulations aimed at determining the pion rejection factor for the proposed configuration of the ALICE TRD with 6 layers. To extract the pion rejection factor we have studied three different methods: i) truncated mean of integrated energy deposit, TMQ; ii) likelihood on integrated energy deposit, L-Q; iii) bidimensional likelihood on energy deposit and position of the largest cluster found in the drift region of the DC, L-QX. Cuts of certain electron efficiency were involved on the likelihood distributions and the pion efficiency is derived within these cuts.

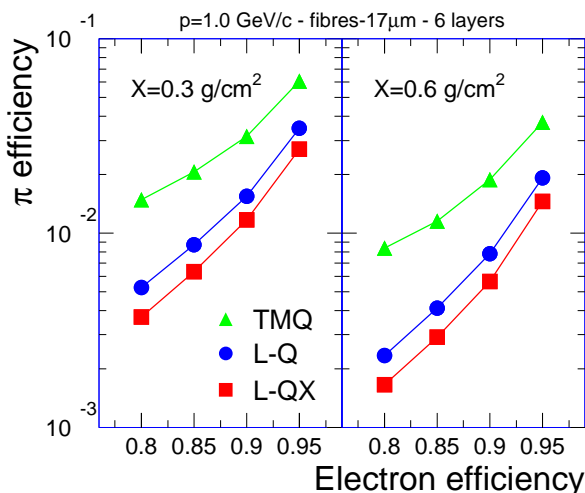


Figure 1: The pion efficiency as function of electron efficiency using the three methods discussed in the text.

In Fig. 1 we present the pion efficiency (the inverse of the rejection factor) as function of electron efficiency (90% electron efficiency is the commonly used value) in case of fibres radiators for the momentum of 1 GeV/c. The three methods introduced above are compared. The truncated mean method, although it delivers sizeably worse identification, has the advantage of being very easy to use, being advantageous especially for an on-line identification. The bidimensional likelihood delivers the best rejection factor.

In general, the three methods employed here give results in good agreement with earlier studies.

By doubling the equivalent thickness of the radiator from $X=0.3 \text{ g/cm}^2$ (left panel of Fig. 1) to $X=0.6 \text{ g/cm}^2$ (right panel) one gains a factor of about 2 in pion rejection power. However, it remains to be seen how the additional material will influence (by producing secondary particles) the performance of the TRD itself and of other ALICE sub-detectors.

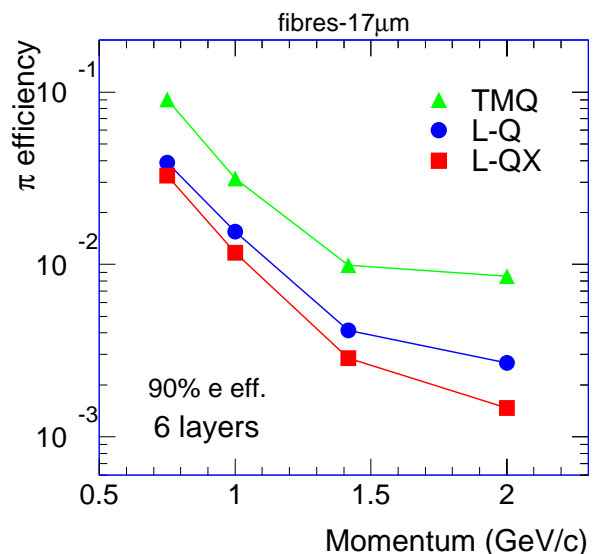


Figure 2: Pion efficiency as function of momentum for a radiator with 17 μm fibres.

The pion efficiency at 90% electron efficiency as function of momentum is shown in Fig. 2. The steep decrease of pion efficiency at momenta around 1 GeV/c is due to the onset of TR production. Towards our highest momentum value, 2 GeV/c, the pion efficiency reaches a saturation, determined by the TR yield saturation and by the pion relativistic rise. Due to these effects the pion rejection is expected to get slightly worse for momenta above 3 GeV/c. As one can see in Fig. 2, at the momentum of 2 GeV/c the pion rejection factor of 300 to 600 achieved during these tests is above the required value for the ALICE TRD. However, one has to bear in mind that a significant worsening of TRD performance has been registered when going from prototype tests to real detectors. This can be the effect of detector loads in a multiparticle environment. On the other hand, impressive pion rejection factors of 1000 and above have been achieved in full size TRDs, i.e. by the HERMES experiment.

References

- [1] TRD Proposal, CERN/LHCC 99-13, available at <http://www.gsi.de/~alice>
- [2] A. Andronic et al., nucl-ex/0102017 (accepted to IEEE Trans. Nucl. Sc.)